國立交通大學

生醫工程研究所

碩 士 論 文

以全域及區域特徵基礎之煙霧偵測

Smoke Detection Using Global and Local Features

研 究 生：彭聖傑

指導教授：林進燈 博士

中 華 民 國 九 十 九 年 七 月

以全域及區域特徵基礎之煙霧偵測
Smoke Detection Using Global and Local Features

研 究 生：彭聖傑　　Student：Shen-Chieh Peng

指導教授：林進燈 博士　　Advisor：Dr. Chin-Teng Lin

國 立 交 通 大 學

生 醫 工 程 研 究 所

碩 士 論 文

A Thesis

Submitted to Institute of Biomedical Engineering

College of Computer Science

National Chiao Tung University

in Partial Fulfillment of the Requirements

for the Degree of Master

in

Computer Science

June 2010

Hsinchu, Taiwan, Republic of China

中華民國 九十九 年 七 月

以全域及區域特徵基礎之煙霧偵測

學生：彭聖傑　　指導教授：林進燈 博士

國立交通大學生醫工程研究所

摘要

本篇論文提出了使用區域特徵分析及全域特徵驗證的煙霧偵測方法，調查中指出近年來基於影像式的煙霧偵測技術在智慧型監控系統中受到廣泛的重視與研究。然而，在一個廣大的開放空間處理煙霧偵測事件如何不被其他常見的干擾物例如行人和車輛所影響，建立一個無誤報的煙霧偵測系統仍是一項具有挑戰性的問題。因此能夠在不同的環境下仍然能找出可區別煙霧以及非煙霧的特徵是一件重要的任務。本篇論文分析影片中每個候選區塊的區域特徵：邊緣模糊化、能量的逐步變化與色彩結構的逐步變化，其中每個區域特徵都對煙霧有足夠的偵測能力以及低誤報。此外，本論文所提出的三種類型的區域特徵都各具互補性，因此，藉由 Boosting 學習演算法加上串聯式架構的方式結合區域特徵以降低更多的誤報。爲了更進一步的克服誤報的情況，提出了全域特徵的統計方式來驗證候選區域的邊緣地帶及整個感興趣移動區域內的資訊。實驗結果指出本篇論文所提出的系統對於不同的環境地點在煙霧偵測上有良好的偵測率以及很低的誤報率以及快速的反應時間。整個系統在執行上具有高效率可對影像做即時處理，並已將此煙霧偵測技術移植到嵌入式系統中。

Smoke Detection Using Global and Local Features

Student: Shen-Chieh Peng Advisor: Dr. Chin-Teng Lin

Institute of Biomedical Engineering
College of
Computer Science
National Chiao Tung University

ABSTRACT

This study presents a novel smoke detection approach using local feature analysis and global feature verification. Studies have investigated visual-based smoke detection techniques in surveillance systems for years. However, given an image in open or large spaces with typical smoke and disturbances of commonly moving objects such as pedestrians or vehicles, detecting smoke without false alarm is still a challenging problem. It is important to find features to distinguish smoke from various environments. This study analyzes characteristics of candidate blocks in video sequences to exploit local features: edge blurring, gradual energy change and gradual color configuration change. Each local feature is strong enough to detect smoke with few false alarms. Moreover, proposed features are complementary to each other. Hence, local features are combined to lower the false alarm rates by boosting cascade architecture. To further overcome some false situation, global feature verification is proposed to gather statistics of information on contour and in the whole area of each candidate region. Experimental results show that the proposed system can well detect

smoke with low false alarm rate within a short reaction time in various environments. The whole system can run in real time and has been implemented on embedded system.

致　　謝

本論文的完成，首先要感謝指導教授林進燈博士這兩年來的悉心指導，讓我學習到許多寶貴的知識，在學業及研究方法上也受益良多。另外也要感謝口試委員們的建議與指教，使得本論文更為完整。

其次，感謝超視覺實驗室的大家長鶴章，還有剛維、建霆、肇廷及東霖、子貴、勝智學長以及 Linda 學姐，提供許多寶貴的意見與耐心的指導。佳芳、健豪、嶸健及哲男同學的相互砥礪，及所有學長、學弟們在研究過程中所給我的鼓勵與協助。尤其是肇廷學長，在研究方法以及論文實驗上給予我相當多的幫助與建議，讓我獲益良多。

感謝我的父母親對我的教育與栽培，並給予我精神及物質上的一切支援，使我能安心地致力於學業。此外也感謝大哥及二哥對我不斷的關心與鼓勵。

謹以本論文獻給我的家人及所有關心我的師長與朋友們。

Contents

List of Tables

List of Figures

Chapter 1

Introduction

1.1 Motivation

In last few years, there were average 5622.8 fire accidents per year according to the report from the National Fire Administration. The number of dead and injured people was nearly 700 and the property loss was about 2 billion NT dollars each year. If the fire accident could be found much earlier, it is more likely to reduce the loss of life and property.

The process of fire development mostly divided into four periods: Ignition, Fire Growth Period, Fully Developed Period and Decay Period as shown in Fig.1-1.

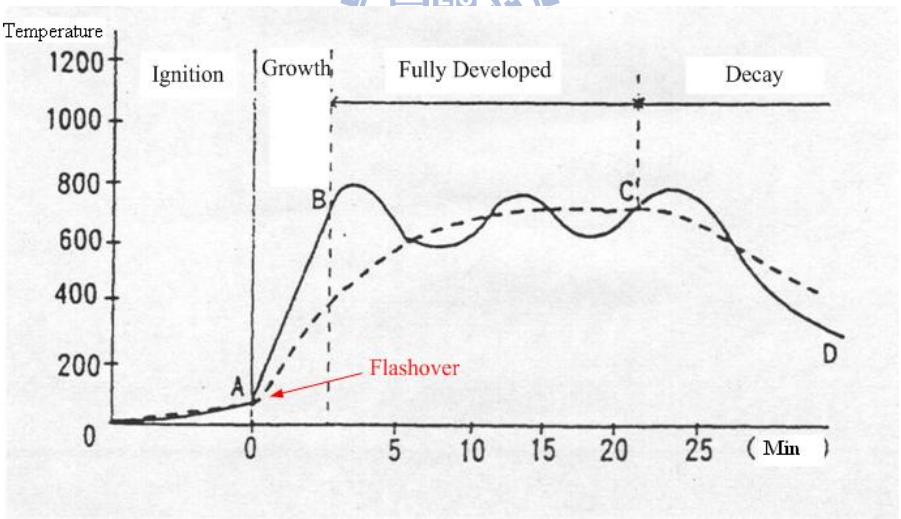

Fig. 1-1 Processing diagram of fire development

In general occurrences of fire, a great quantity of thick smoke instead of fire is produced in the initial stage. After flashover, fire spreads quickly and burns all spaces continuously. Therefore, the beginning of fire can be observed soon before it causes any real damage.

Conventional point-based sensors typically detect the presence of smoke particles by ionization or photometry. These detectors rely on the smoke propagation to a fixed point and therefore cannot operate in large or open spaces, such as hangers, tunnels, storage facilities, and offshore platforms. Moreover, conventional sensors inherently suffer from the transport delay of the smoke from the fire to the sensor [10]. Many researchers have recently investigated video smoke detection (VSD) that may address problems in point-based sensors. However, development of video smoke detection is still in an early stage due to the difficulty in modeling and characterizing smoke by primitive visual features such as intensity, motion, and edge. In last study, our system achieves the goal of high detection rate and short reaction time with lower false alarm rate. In last study, researchers proposed block based computation to improve the performance, using wavelet energy ratio to analyze the gradual energy change and the color configuration change. However, combining each local feature still not overcome some critical problems such like huge tourist coaches, light reflection with a big area, etc. As same as the goal of last study, researchers attempt to improve the false alarm rate while keeping a high detection rate and short reaction time. This study, researchers applied the concept of boosting and cascade architecture to combine the local features. This occurrence, optimizing the features combination automatically and lower the computation time. In addition, adding the global features to make the system more stability.

1.2 Related Work

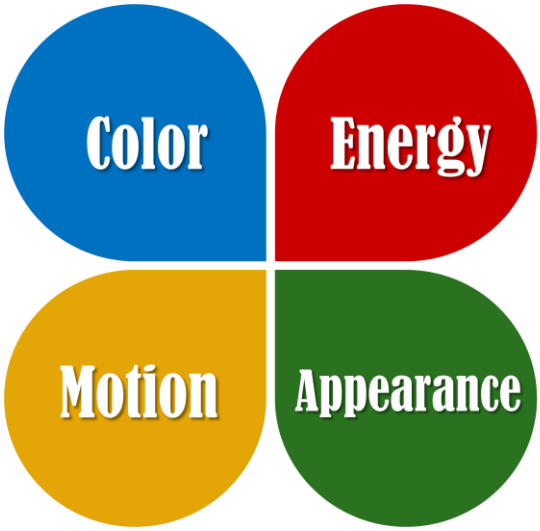

Fig. 1-2 Four categories of video smoke detection

Features used for smoke detection can be divided into four categories: motion, appearance, color, and energy (texture) as shown in Fig. 1-2. The first category includes *Motion-Based* approaches [1, 3-4, 21]. Vicente et al. [1] discriminate distant smoke from other phenomena by extracting the transitory and complex motion. Kopilovic et al. [3] observed irregularities in motion due to non-rigidity of smoke. Yuan et al. [4] proposed a fast orientation model that produces a more effective way to extract motion characteristics.

The second category includes *Appearance-Based* approaches [2, 5-11]. Toreyin et al. [2] indicated that smoke from an uncontrolled fire expands in time and results in regions with convex boundaries. Chen et al. [5] found that airflows change the shape of smoke in various ways at any time, and introduced a disorder measure, the ratio of circumference to area for the extracted smoke region, to analyze shape complexity. Moreover, incremental smoke pixels are calculated to obtain the growth-rate to characterize the diffusion process of smoke. Yang et al. [6] analyzed the changing

unevenness of density distribution and the changing irregularities of the contour of smoke. Fujiwara et al. [9] extracted smoke regions from an image using fractal encoding concept.

Color-Based approaches [2, 5, 11-14, 21, 22] comprise the third category. Smoke pixels gradually change the color configuration. Smoke typically displays grayish colors during the burning process [5]. A particle filter coped with multi-model probability density function (pdf) was implemented for 3D color representation [12]. Independent of fuel type, smoke naturally decreases chrominance channels U and V of YUV color space in the candidate region [2]. Kim et al. [24] used the temporal information of its color and shape extracted from the regions of interest (ROI) to decide whether the ROI is smoke or not.

The fourth category includes *Energy-Based* approaches [2, 13-23]. Lai et al. Wavelet coefficients contain high frequency information of the original image [17]. Since smoke obstructs the texture and edges in the background of an image [2], a decrease in wavelet energy is an important clue for smoke detection. Piccinini et al. [16] further improve the concept by on-line modeling the ratio between the current input frame energy and the background energy.

None of features is perfect. Each feature has false alarms in certain cases such as a vivid person with grayfish clothes, presences of huge tourist coaches, trees with vivid leafs and shadow, and background with poor textures. Current researches combined various features to lower the false alarm rate [11, 21, 22]. In this paper, spatial and temporal analyses based on block processing are proposed to enhance smoke features. Energy-based and color-based features are analyzed in spatial, temporal, and spatial-temporal domains. Proposed system further combined the local features with the global features. Local features are combined by boosting cascade architecture. Global feature verification consists of area ratio, contour analysis and

region analysis. The proposed system ran more than six hours in various conditions to verify fire safety reliability in the real world. Experimental results show that the proposed system can detect smoke with low false alarm rate within a short reaction time.

1.3 Thesis Organization

The remainder of this thesis is organized as follows. Chapter 2 describes the proposed system architecture and grid-processing including background modeling, and candidate selection. Chapter 3 presents local feature analysis. Chapter 4 presents classification and global feature verification. Chapter 5 describes the experimental results and discussions. Finally, draws conclusions and future work will be presented in chapter 6.

Chapter 2
System Architecture and Grid-Processing

2.1 System Architecture

Figure 2-1 shows the system architecture of the proposed video smoke detection (VSD) technique, including three processing units: the grid- processing unit, the local feature classification unit and the global feature verification unit. The rest of this chapter focuses on the details of the grid processing unit.

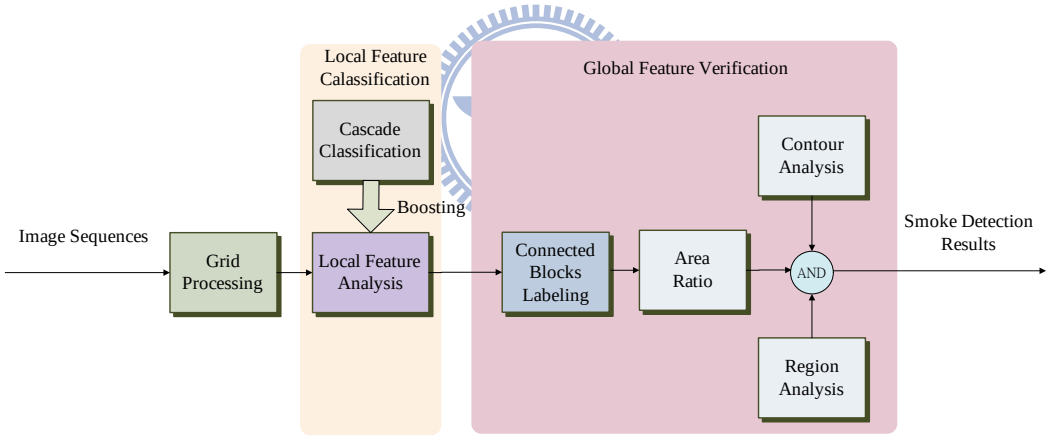

Fig. 2-1 System architecture

2.2 Grid Processing

Figure 2-2 depicts the flow chart of the grid processing unit. The input is gray level image sequences, and the output is candidate grid with moving property. Two common methods are used for obtaining the foreground image. One is temporal difference and the other is background subtraction. The temporal difference method

can be implemented by subtracting frame *t-1* from frame *t*, and the regions with an obvious intensity variation are considered as the foreground region. Background subtraction is also a similar method, but this work uses a constructed background image instead of frame *t-1*. This work applied the Gaussian Mixture Model (GMM) [25] to construct background. This technique models each pixel as a Gaussian mixture and uses an on-line EM algorithm to update the model. This technique deals properly with lighting changes, repetitive motion from clutter, and long-term scene changes.

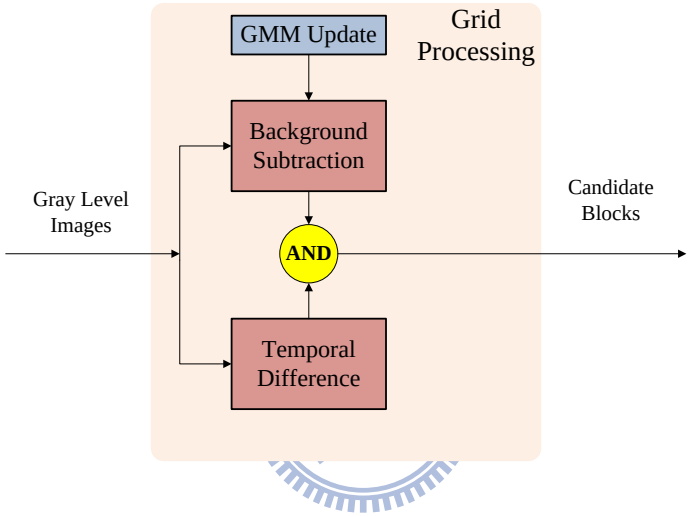

Fig. 2-2 Grid processing

To temporally analyze smoke, tracking smoke target by foreground segmentation is a necessary step for object-based approach. However, smoke regions appear and disappear frequently because of the special particle property during ignition and combustion as Fig. 2-3 shows. Tracking or analyzing the smoke target using an object-based method is inefficient. A block-based technique can solve this problem. The block-based system only needs to check the presence of smoke inside the block, and therefore can temporally analyze features belong to each block in the screen.

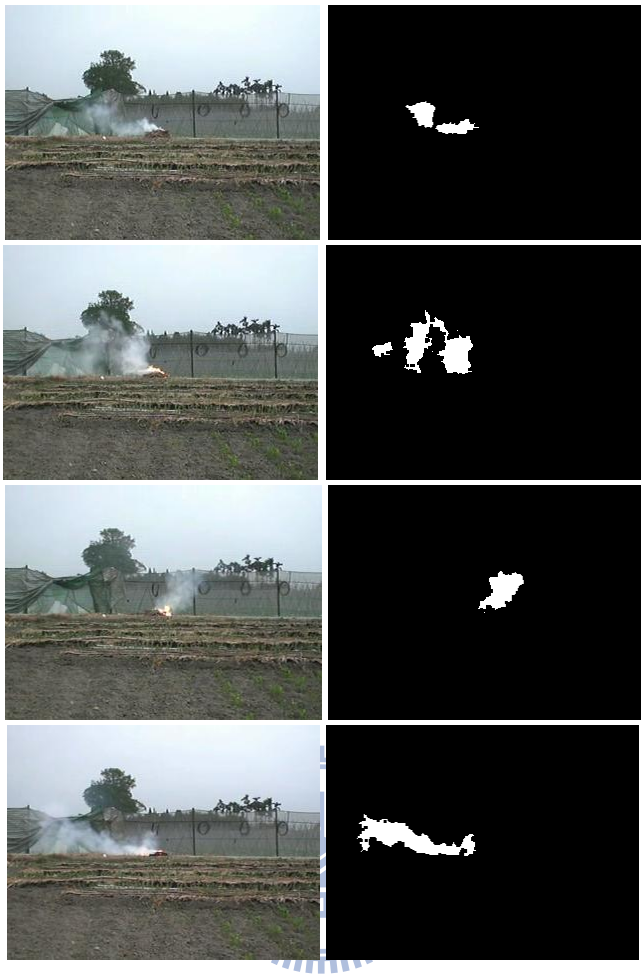

Fig. 2-3 Smoke regions appear and disappear continuously

2.2.1 Background Modeling

Gaussian Mixture Model (GMM) [25] is a common and robust method in background construction, and we choose GMM to build the background image. It will be described as follows.

Generally speaking, the intensity of each pixel varies in a small interval except the region of foreground objects. It is proper to use a Gaussian model to construct the background image. But in many surveillance videos, we would observe that there are waving leaves, sparking light, etc. In these situations, some background pixels would vary in several specific intervals. In other words, using two, three or more Gaussian

distributions to model a pixel will obtain a better performance. This study presents the flow chart of GMM background construction in Fig. 2-4.

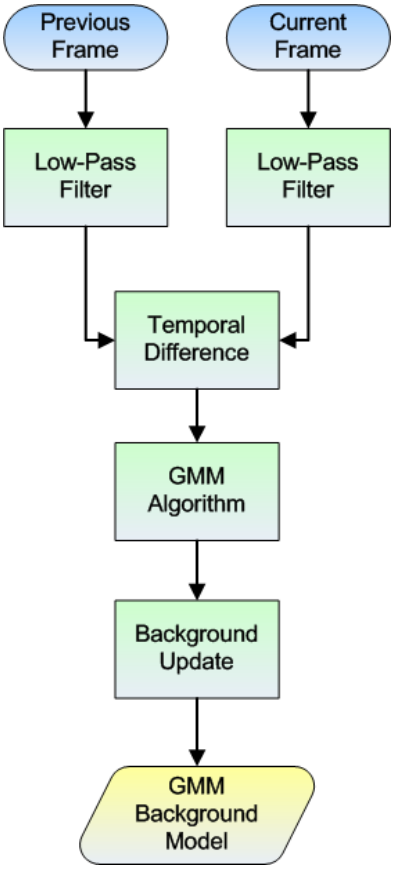

Fig. 2-4 GMM background model construction

Firstly, low-pass filter will be employed to reduce the noise. The GMM method models intensity of each pixel with K Gaussian distributions. The probability that a certain pixel has a value of X_t at time *t* can be written as Eq. (2.1)

$$P(X_t) = \sum_{k=1}^{K} \omega_{k,t} \cdot \eta(X_t, \mu_{k,t}, \sum_{k,t}) \tag{2.1}$$

where K is the number of distributions that we used, $\omega_{k,t}$ represents the weight of *k*-th Gaussian in the mixture at time *t*, $\mu_{k,t}$ is the mean of *k*-th Gaussian in the mixture at time *t*, $\sum_{k,t}$ is the covariance matrix of the *k*-th Gaussian in the mixture at time *t*, and η is a Gaussian probability density function shown in Eq. (2.2).

$$\eta(X_t, \mu_t, \sum_t) = \frac{1}{(2\pi)^{n/2} |\sum_t|^{1/2}} \exp\{-\frac{1}{2}(X_t - \mu_t)^T \sum_t^{-1}(X_t - \mu_t)\} \quad (2.2)$$

where n is the dimension of data. In order to simplify the computation, it assumed that each channel of data are independent and have the same variance, and then can assume the covariance matrix as Eq. (2.3).

$$\sum_{k,t} = \sigma_k^2 \mathrm{I} \quad (2.3)$$

Temporal difference is applied to extract the possible background regions, and update pixels inside these regions. Then, sorting Gaussian distributions by the value of ω/σ, and choose the first B distributions to be the background model, i.e. shown as Eq. (2.4).

$$B = \arg\min_b (\sum_{k=1}^{b} \omega_{k,t} > T) \quad (2.4)$$

When a new pixel is inputted (intensity is X_{t+1}), it will be checked against the K distributions by turns. If the probability value is within 2.5 standard deviations, and this pixel is considered as background. Then, we update weight, mean, variance by Eq. (2.5), (2.6), (2.7).

$$\omega_{k,t+1} = (1-\alpha)\omega_{k,t} + \alpha(M_{k,t+1}) \quad (2.5)$$

$$\mu_{t+1} = (1-\rho)\mu_t + \rho X_{t+1} \quad (2.6)$$

$$\sigma_{t+1}^2 = (1-\rho)\sigma_t^2 + \rho(X_{t+1} - \mu_{t+1})^T (X_{t+1} - \mu_{t+1}) \quad (2.7)$$

where α is a learning rate, $M_{k,t+1}$ is 1 for the model which matched and 0 for remaining models, and Eq. (2.8) shows the second learning rate ρ.

$$\rho = \alpha\eta(X_{t+1} | \mu_{k,t}, \sigma_{k,t}) \quad (2.8)$$

Besides, the remaining Gaussians only update the weight. If there is no any distribution is matched, we replace the mean, variance and weight of the last distribution by X_{t+1}, a high variance and a low weight value, respectively.

Figure 2-5 shows the constructed background image by GMM. Figure 2-6 shows the foreground image obtained by background subtraction.

(a) Video sequence (b) GMM Background Image

Fig. 2-5 Background image construction by GMM

(a) Current image (b) Foreground image

Fig. 2-6 Foreground image obtained by background subtraction

2.2.2 Candidate Selection

The image will be divided into non-overlapped blocks, and each block has the same size in a same image. To find out the moving block with a gray-level change, the foreground image will be obtained by GMM approach, and the sum of foreground image for each pixel as shown in Eq. (2.9)

$$S_k = \begin{cases} 1, & if \left| \sum_{x,y \in S_k} \left[foreground(x,y,t) \right] \right| > T_1 \\ 0, & otherwise \end{cases} \tag{2.9}$$

where S_k is the k^{th} block and *x, y* is the coordinates of the scene. T_1 is the predefined threshold.

Foreground regions can be found by the GMM approach, but they could also include static objects. Consequently, temporal difference of two successive frames will be employed. All pixels in the difference image with value "1" are considered as moving objects in the scene. To reduce the disturbance of noises, the temporal block difference is computing the summation for each block to determine the moving property defined by Eq. (2.10).

$$T_k = \begin{cases} 1, & if \left| \sum_{x,y \in T_k} \left[f(x,y,t) - f(x,y,t-\Delta t) \right] \right| > T_2 \\ 0, & otherwise \end{cases} \tag{2.10}$$

where T_k is the k^{th} block and *x,y* is the coordinates of the scene, *f* is the input image and T_2 is the predefined threshold.

To reduce computational cost, only values of background subtraction and temporal difference larger than the predefined thresholds will be regarded as candidates containing moving objects by Eq. (2.11) and Figure 2-7 shows the results of "grid processing".

$$B_k = \begin{cases} 1, & if\ S_k\ AND\ T_k = 1 \\ 0, & otherwise \end{cases} \tag{2.11}$$

Fig. 2-7 Results of grid processing

Chapter 3

Local Feature Analysis

This chapter will be divided into three parts according to three different kind of local feature analysis. Firstly, based on the smoke will blur the scene, comparing the energy of background with foreground is proposed in this paper. Furthermore, analyzing one-dimension temporal wavelet energy by different from the other physical objects, smoke will change the energy of scene smoothly. Finally, as same as the last feature, smoke will change the color configuration much smooth than the other objects. All of the local features are based on block based processing.

3.1 2-D Spatial Wavelet Analysis

Although the Fourier transform has been the mainstay of transform-based image processing since the late 1950s, a more recent transformation, called the wavelet transform, is now making it even easier to compress, transmit, and analyze many images. Unlike the Fourier transform, whose basis functions are sinusoids, wavelet transforms are based on small waves, called wavelets, of varying frequency and limited duration. This allows them to provide the equivalent of a musical score for an image, revealing not only what notes (frequencies) to play but also when to play them. Conventional Fourier transforms, on the other hand, provide only the notes or frequency information; temporal information is lost in the transform process.

Now we want to transform an image (M by N) into wavelet domain. The whole 2-D spatial wavelet transform can be decomposed by the horizontal wavelet transform and the vertical wavelet transform. Fig. 3-1 is the diagram of horizontal wavelet

transform. The direction from left to right is the wavelet decomposition, and the direction from left to right is the wavelet synthesis.

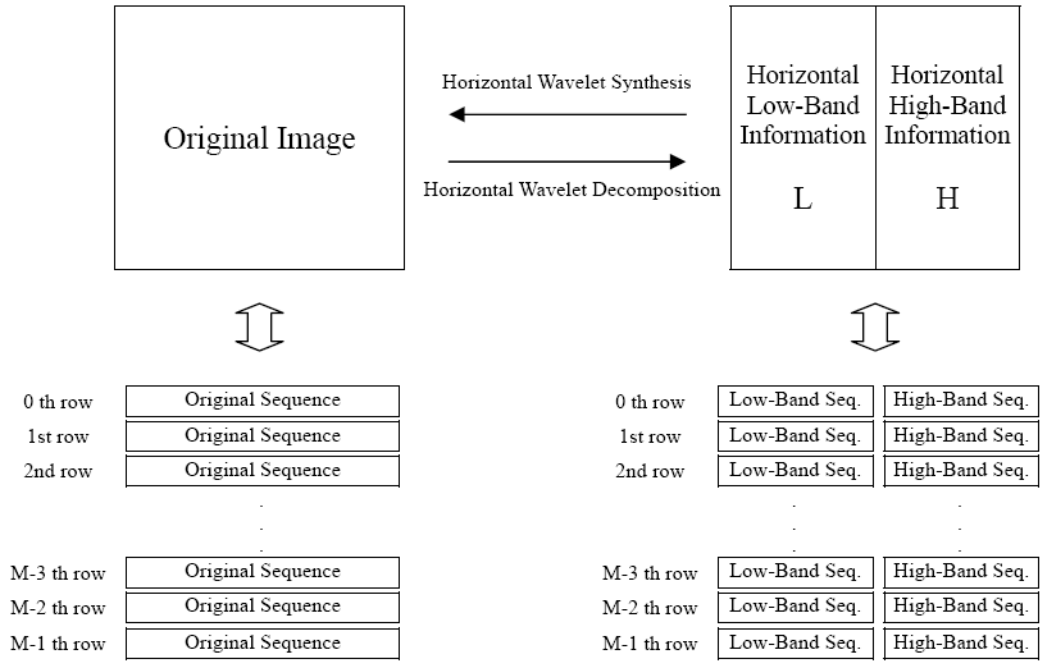

Fig. 3-1 Horizontal wavelet transformation

Each row of the image will be regarded as mutual independent image sequences and each independent row will process wavelet transform respectively. Briefly, a original image will be decomposed into low-band information on the left side and high-band information on the right side after horizontal wavelet transform. We used L and H stand for low-band and high-band information, respectively.

Vertical wavelet transform will process on L and H obtained by horizontal transforms and the whole wavelet transform will be done. Fig. 3-2 is the diagram of vertical wavelet transform. The direction from left to right is the wavelet decomposition, and the direction from right to left is the wavelet synthesis. The data on the left side was processed by horizontal wavelet transform but not vertical wavelet transform yet. Each column of the image will be regarded as mutual independent image sequences and each independent column will process wavelet

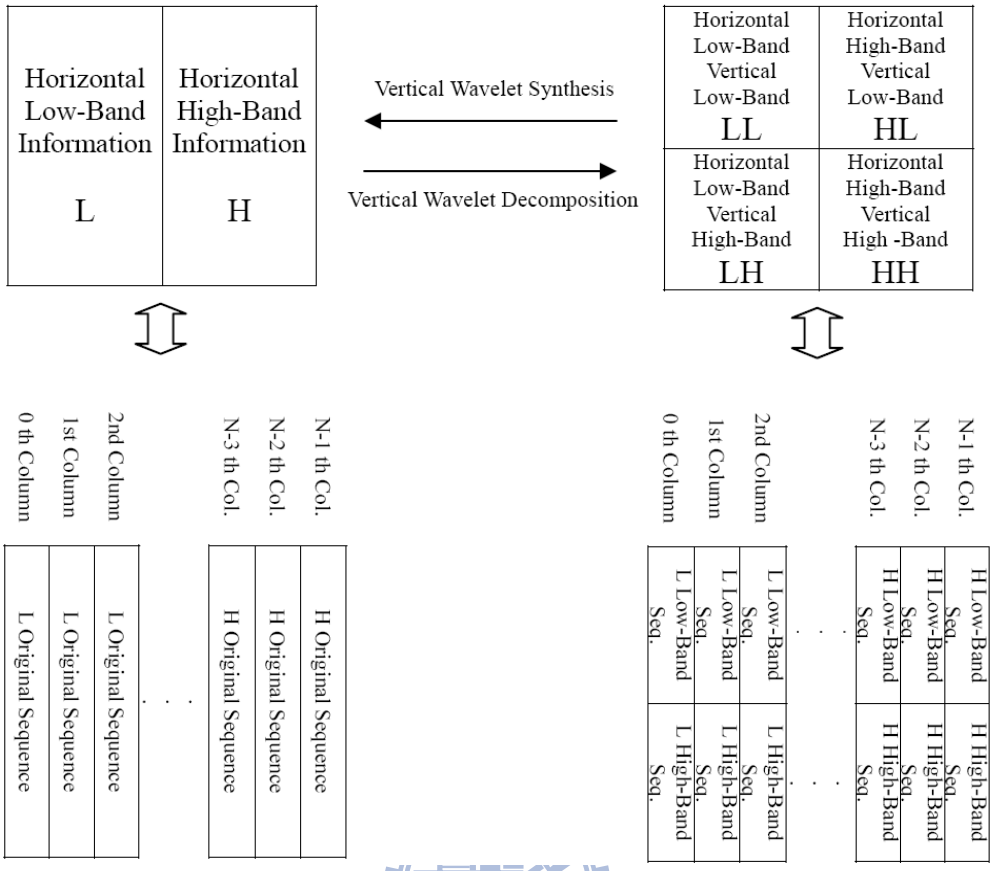

Fig. 3-2 Vertical wavelet transformation

transform, respectively. Anyhow, the data can further separate into upside and underside after vertical wavelet transform. The upside is the vertical low-band information and the underside is the vertical high-band information as shown on the right side of Fig. 3-2. To operate in coordination with horizontal transform, the whole image data can separate into four regions, which are horizontal low-band vertical low-band (LL), horizontal low-band vertical high-band (LH), horizontal high-band vertical low-band (HL), and horizontal high-band vertical high -band (HH).

It is well-known that wavelet subimages contain the texture and edge information of the original image. Edges produce local extreme in wavelet subimages [15]. Wavelet subimages LH, HL, and HH contain horizontal, vertical and diagonal high frequency information of the original image, respectively. Fig. 3-3 is the original image and its single level wavelet subimages.

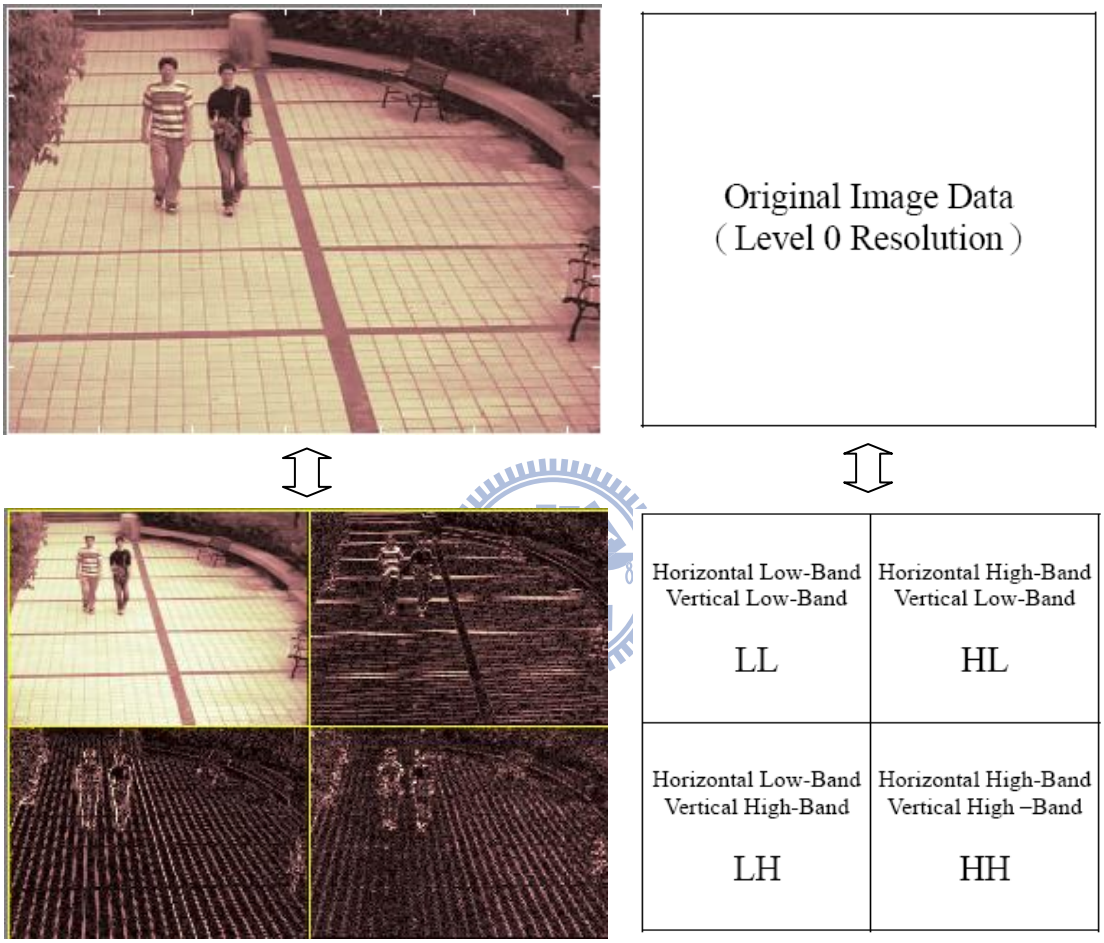

Fig. 3-3 Original image and its single level wavelet subimages

Because smoke blurs the texture and edges in the background of an image, high-frequency information becomes much more invisible when smoke covers part of the scene. Therefore, details will be an important indicator of smoke due to the decrease in value of high-frequency information. Energy of details is calculated for each candidate block:

$$E(B_k, I_t) = \sum_{x,y \in B_k} \left[LH(x,y)^2 + HL(x,y)^2 + HH(x,y)^2 \right] \tag{3.1}$$

where B_k is the k^{th} block of the scene, I_t is the input image at time t and the wavelet transform coefficients are shown in Fig. 3-4.

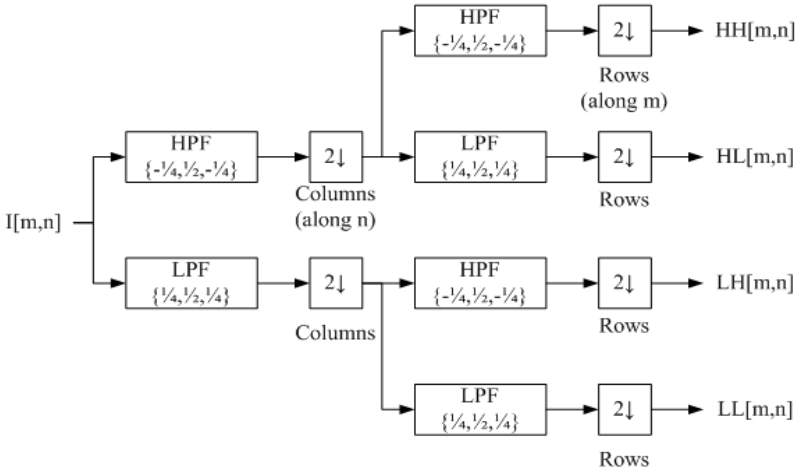

Fig. 3-4 Two-dimension wavelet transform and its coefficients

Instead of using energy of the input directly, we prefer computing the energy ratio of the current frame to the background model due to the cancelation of negative effect on different conditions and the capability of impartial measurement in the decrease:

$$\alpha(B_k, t) = \frac{E(B_k, I_t)}{E(B_k, BG_t)} \tag{3.2}$$

where BG_t is the mean value of the distribution with a highest weight in the GMM background model. The value of the energy ratio α is our first feature in spatial domain, which supports the fact that the texture or edges of the scene observed by the camera are no longer visible as they used to be in the current input frame. It is also possible to determine the location of smoke using the wavelet subimages as shown in Fig. 3-5.

(a) Original frame without smoke

(b) Frame with smoke

Fig. 3-5 Blurring in the edges is visible by single level wavelet subimages

3.2 1-D Temporal Energy Analysis

A wave is an oscillating function of time or space and is periodic. In contrast, wavelets are localized waves. They have their energy concentrated in time or space and are suited to analysis of transient signals. Differential signal is easy to extract the suddenly change of signals and the computation cost is lower to anther analysis methods. In figure 3-6 shows the original signal and the differential signal. It is an applicable way to calculate the quantity of changing value.

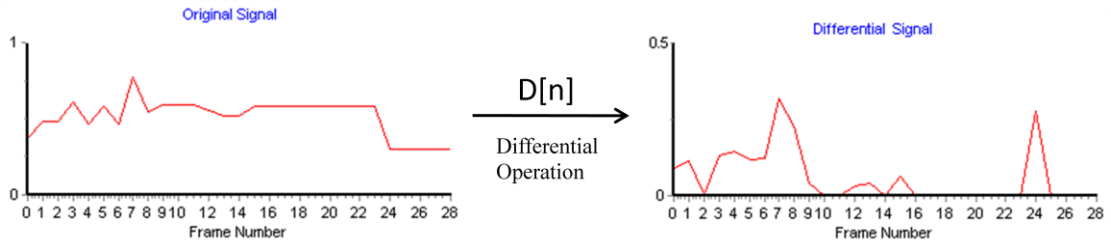

Fig. 3-6 Block diagram of 1-D differential operation

Ordinary moving objects such as pedestrians or vehicles have solid characteristic so we can't see details behind through the bodies. If there is an ordinary moving object going through the candidate block then there will be a sudden energy change because of the transition from the background to the foreground object. On the contrary, initial smoke has semi-transparent nature and becomes less visible as time goes by.

A gradual change of energy is guaranteed to this process and any abrupt variation will be regarded as a noise caused by common disturbance. One-dimension temporal differential analysis of energy ratio α provides a proper evaluation of this phenomenon. We obtain variation information by the 1-D differential shown in Fig.3-6. Therefore, the disturbance can be measured by computing the summation of variations for a predefined time interval. Obviously, ordinary solid moving objects produce a great quantity of variations in Fig. 3-7(b). Smoke has smooth variation in value of energy ratio and produces few variations shown in Fig. 3-7(e). The likelihood of the candidate block to be a smoke region is in inverse proportion to the parameter β

$$\beta_E(B_k,t)=\frac{\sum_{n=t-N}^{t}\left|D_\alpha[n]\right|}{N} \tag{3.3}$$

where D[n] is the differential signal information of energy ratio α and t is current frame and N is the number of calculate frame.

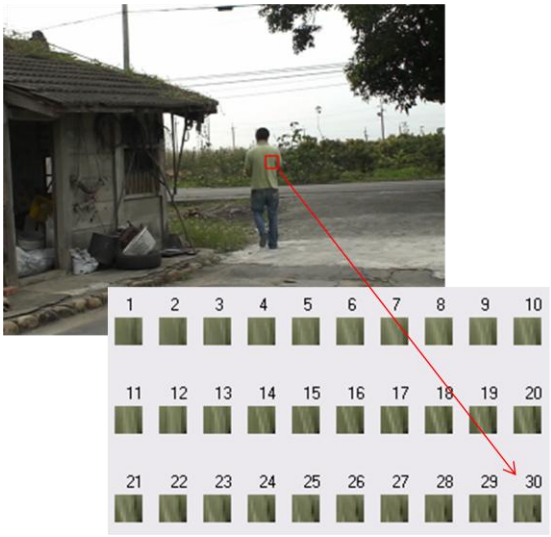
1 2 3 4 5 6 7 8 9 10
11 12 13 14 15 16 17 18 19 20
21 22 23 24 25 26 27 28 29 30

(a)

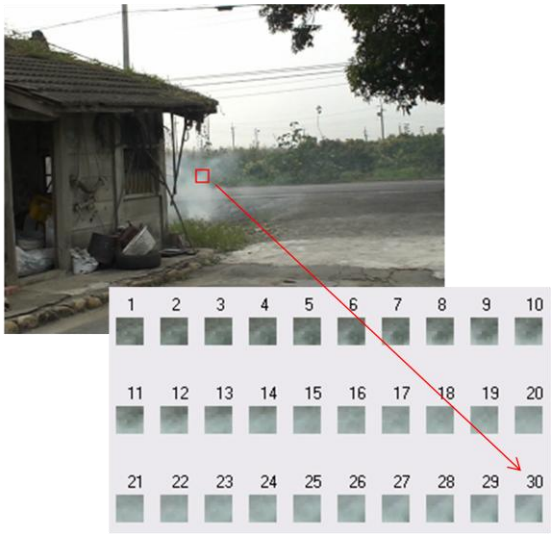
1 2 3 4 5 6 7 8 9 10
11 12 13 14 15 16 17 18 19 20
21 22 23 24 25 26 27 28 29 30

(d)

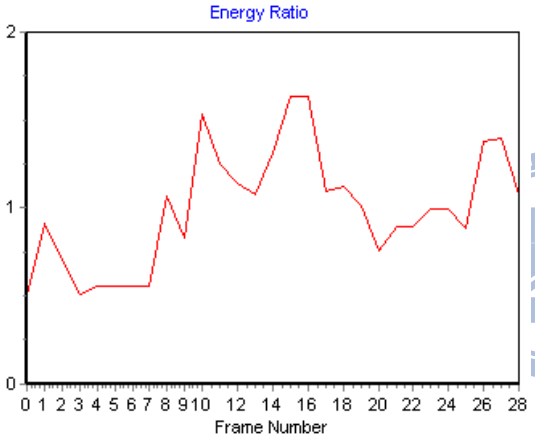
Energy Ratio
2
1
0
0 1 2 3 4 5 6 7 8 9 10 12 14 16 18 20 22 24 26 28
Frame Number

(b)

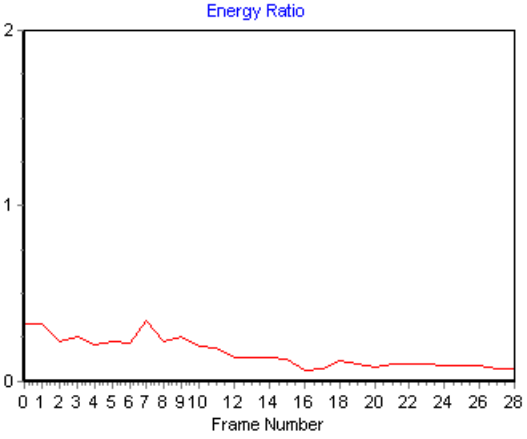
Energy Ratio
2
1
0
0 1 2 3 4 5 6 7 8 9 10 12 14 16 18 20 22 24 26 28
Frame Number

(e)

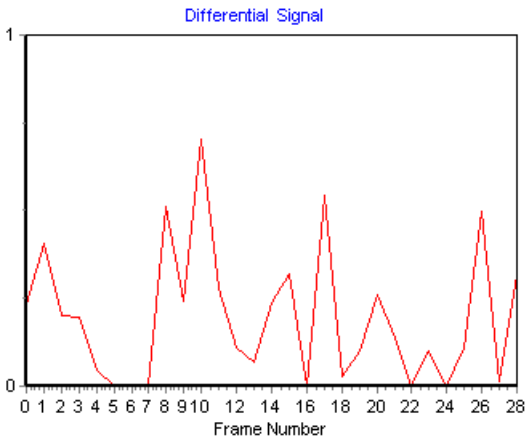
Differential Signal
1
0
0 1 2 3 4 5 6 7 8 9 10 12 14 16 18 20 22 24 26 28
Frame Number

(c)

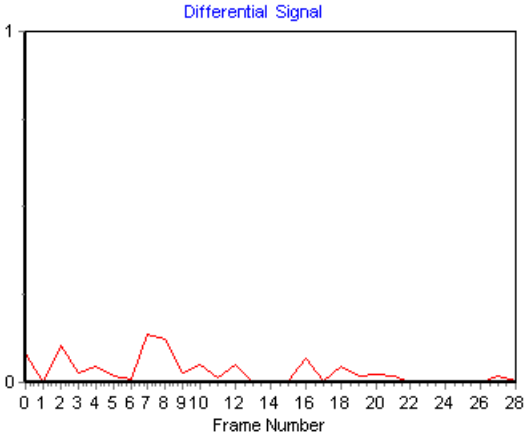
Differential Signal
1
0
0 1 2 3 4 5 6 7 8 9 10 12 14 16 18 20 22 24 26 28
Frame Number

(f)

Fig. 3-7 Comparison of changes on the wavelet energy ratio at the passage of an ordinary moving object and smoke objects. (a) Sample frame from the test sequence and temporal candidate block with an ordinary moving object. (b) Profile of the wavelet energy ratio in the selected block. (c) Differential signal of the wavelet energy ratio in the same block with possible observation of sudden change properties. (d) Sample frame from the test sequence and temporal candidate block with smoke objects. (e) Profile of the wavelet energy ratio in the selected block. (f) Differential signal of the wavelet energy ratio in the same block, with possible observation of gradual change properties.

3.3 1-D Temporal HSV Analysis

Smoke is hard to be defined by a specific color appearance precisely. However, it is possible to characterize smoke by considering its effect on the color appearance of the region on which it covers. Besides the gradual change of energy, smoke has the same property of color configuration.

Color analysis is performed in order to identify those pixels in the image that respect chromatic properties of smoke. The HSV color space and photometric invariant features are considered in the analysis. Photometric invariant features are functions describing the color configuration of each image coordinate discounting local colors variations. HSV stands for hue, saturation, and value, and is also often called HSB （B for brightness）. HSV color space describes in figure 3-8. A third model, common in computer vision applications. HSV is the most common cylindrical-coordinate representations of points in an RGB color model, which rearrange the geometry of RGB in an attempt to be more perceptually relevant than the cartesian representation and the full spectrum of colors can be created by edit these three values：

Hue is another word for color. Red, blue, and yellow are the primary hues, and

when combined in equal amounts they create the secondary hues orange, green and violet. However, moving around the cone changes the Hue color along the rainbow.

Saturation is the intensity of a color (or hue). Mix colors or add black to a color, saturation and intensity drops. Add white, color becomes lighter, but not necessarily more intense. The colors are more pure when the S (saturation) values increasingly.

Value is the lightness of a color. Like saturation, adding black or white to a color affects value. Tints are colors with added white, and shades are colors with added black.

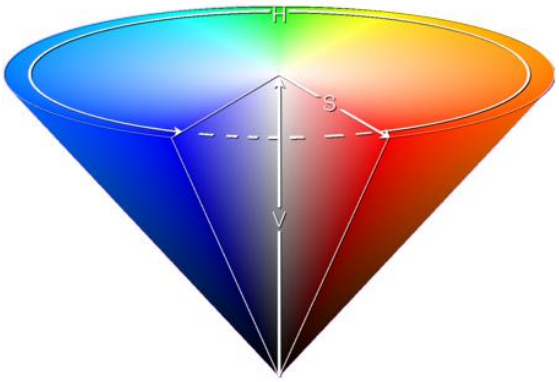

Fig. 3-8 HSV color space

It is often more natural to think about a color in terms of hue and saturation than in terms of additive or subtractive color components. They were developed in the 1970s for computer graphics applications, and are used for color pickers, and for image analysis and computer vision. Hue and saturation in the HSV color space and the normalized-RGB color space are two photometric invariant features in common use.

This work uses the HSV color space for its fast computation since it can be obtained by each channel. From the empirical analysis, smoke smooth changes each component in HSV color space of the covered point but smoke doesn't severely change the configuration of the *HSV* color system. However, the configuration is likely to change in case of a material change. This constrain can be represented by

$$
\begin{aligned}
H\left(B_k,t\right) &\cong H\left(x,y,t+\Delta t\right) \\
S\left(B_k,t\right) &\cong S\left(x,y,t+\Delta t\right) \\
V\left(B_k,t\right) &\cong V\left(x,y,t+\Delta t\right)
\end{aligned} \tag{3.4}
$$

This investigation draws the HSV color histogram of a specific block in three different situations of a video sequence in order to characterize the presence or absence of smoke. The color histogram distribution in Fig. 3-9 (c) is similar to the one in Fig. 3-9 (a). However, the presence of pedestrian produces totally different color histogram distributions between Fig. 3-9 (b) and Fig. 3-9 (a).

(a)

(b)

(c)

Fig. 3-9 HSV color histogram of a specific block (a) original image (b) covered by ordinary moving objects (c) covered by smoke

Variations of the three channels in the HSV color system are obtained by the 1-D differential again in Fig. 3-10. Ordinary solid moving objects produce a great quantity of variations in the right column of Fig. 3-10 (b). Smoke has smooth variation in HSV color space and produces few impulses shown in the right column of Fig. 3-10 (d).

$$\beta_H(B_k,t)=\frac{\sum_{n=t-N}^{t}|D_H[n]|}{N}$$
$$\beta_S(B_k,t)=\frac{\sum_{n=t-N}^{t}|D_S[n]|}{N} \quad (3.5)$$
$$\beta_V(B_k,t)=\frac{\sum_{n=t-N}^{t}|D_V[n]|}{N}$$

Where $D_H[n]$, $D_S[n]$, and $D_V[n]$ stand for differential signal of *H*, *S* and *V* channels respectively. The likelihood of the candidate block to be a smoke region is in inverse proportion to the parameter β.

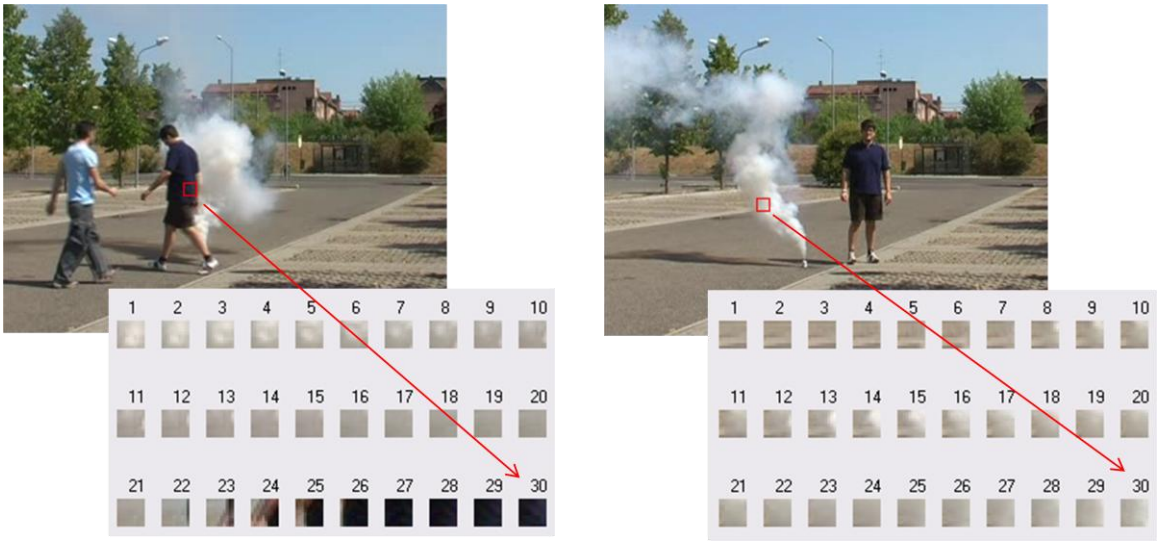

(a) (c)

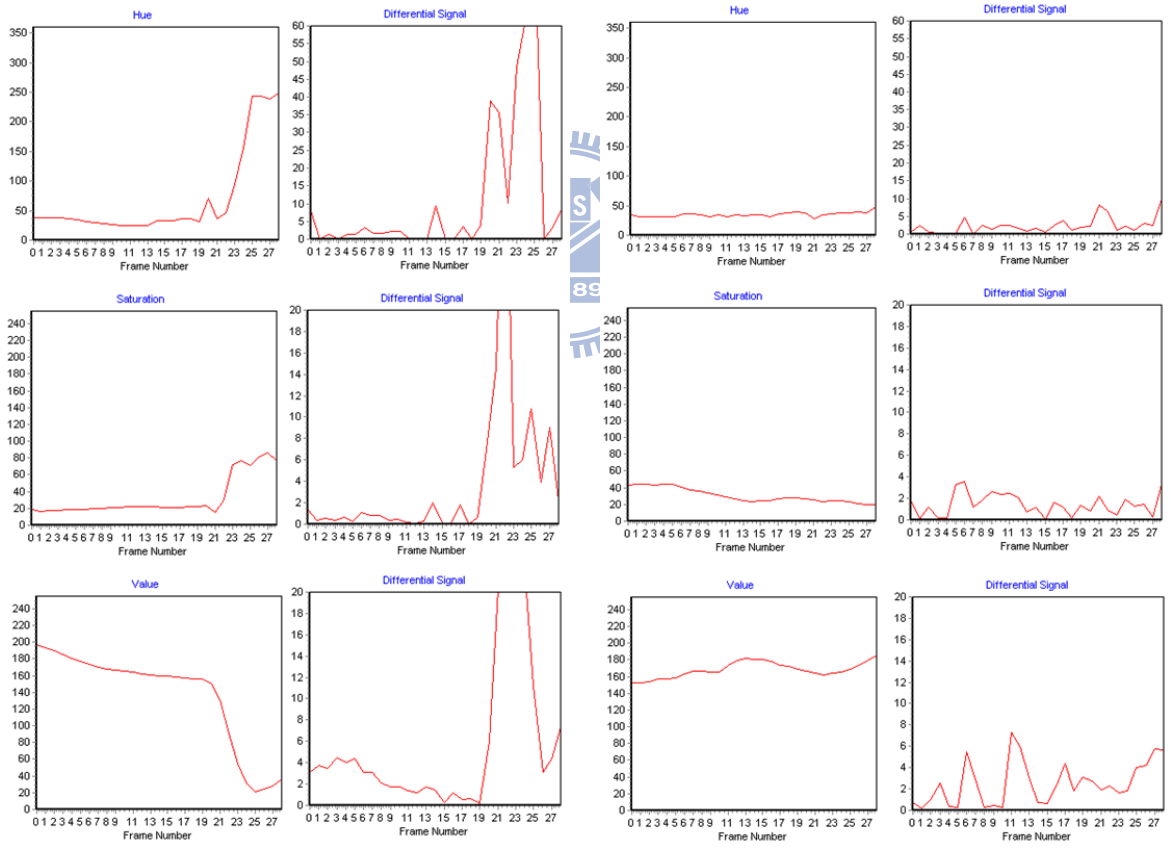

(b) (d)

Fig. 3-10 Comparison of changes on color components of HSV color spaces at the passage of an ordinary moving object and smoke objects. (a) Sample frame from the

test sequence and temporal candidate block with an ordinary moving object. (b) Left column profile of the H, S and V color components in the selected block and right column profile of the differential signal of H, S and V components in the same block with possible observation of variance properties. (c) Sample frame from the test sequence and temporal candidate block with smoke objects. (d) Left column profile of the H, S and V color components in the selected block and right column profile of the differential signal of H, S and V components in the same block with possible observation of invariance properties

Chapter 4

Classification and Verification

This chapter will be divided into two parts. First part will introduce the classifier of this system. Five features proposed in the previous chapter are partially complementary with different physical meanings. The 2-D spatial wavelet feature α in chapter 3.1, distinguish high-texture objects from smoke. The 1-D temporal energy feature β_E in chapter 3.2, distinguishes objects suddenly change the texture in the candidate block. The 1-D temporal chromatic configuration feature β_H, β_S and β_V in chapter 3.3, distinguishes objects suddenly change the color structure in the candidate block. In this section, five proposed features are combined as feature vector $x = [\alpha, \beta, \rho]$ $x = [\alpha, \beta_E, \beta_H, \beta_S, \beta_V]$ for each candidate block and classified by cascade classifier. Second part of this chapter will introduce the global feature verification in this system. There are three verification processes: area ratio, contour analysis and region analysis and they are also proposed to further reduce the false alarm rate.

4.1 Classification

The conventional AdaBoost [26] procedure can be easily interpreted as a greedy feature selection process. Consider the general problem of boosting, in which a set of classification functions are combined using a weight majority vote. The challenge is to associate a large weight with each good classification function and a smaller weight with poor functions. AdaBoost is an aggressive mechanism for selecting a small set of good classification functions which nevertheless have significant variety. This study, researchers proposed five features that introduced in previous chapter and the threshold

selection for each feature is described in below.

For distribute the information of each value for block-based smoke database. To find a threshold that determines the optimal threshold classification function, causing the minimum number of examples are misclassified. Eq. (4.1) is a weak classifier $h(x, f, p, \theta)$ consists of a feature (f), a threshold (θ) and a polarity (p) indicating the direction of inequality. Here x is a 10x10 pixels image.

$$h(x, f, p, \theta) = \begin{cases} 1, \ if \ pf(x) < p\theta \\ 0, \ otherwise \end{cases} \tag{4.1}$$

Figure 4-1 is the flow chart of optimal threshold selection for each feature. Selected threshold of each feature is trained by block-based smoke 10x10 patch database which consists of 2,336 smoke images and 23,632 non-smoke images.

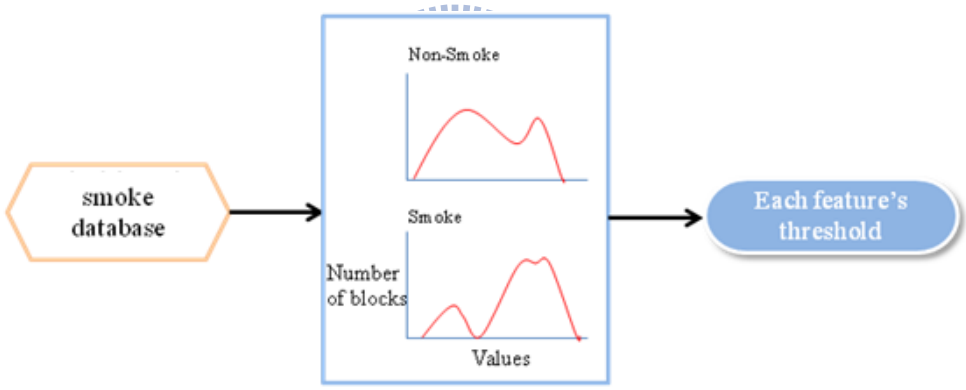

Fig. 4-1 Optimal threshold selection for each feature

The algorithm described in Table 4-1 is used to select key weak classifiers form the set of possible weak classifiers. In this study case, five local features are proposed to classify smoke blocks and non-smoke blocks. In this study case, all of the weak classifiers (five local features) introduced in last chapter.

Table 4-1 Boosting algorithm for learning a query online

T hypotheses are constructed each using a single feature. The final hypothesis is a weighted linear combination of the T hypotheses where the weights are inversely proportional to the training errors.

- Given example images $(x_1, y_1), \ldots, (x_n, y_n)$ where $y_i = 0, 1$ for negative and positive examples respectively.
- Initialize weights $w_{1,i} = \frac{1}{2m}, \frac{1}{2l}$ for $y_i = 0, 1$ respectively, where m and l are the number of negatives and positives respectively.
- For $t = 1, \ldots, T$:
  - Normalize the weights,

$$w_{t,i} \leftarrow \frac{w_{t,i}}{\sum_{j=1}^{n} w_{t,j}}$$

  - Select the best weak classifier with respect to the weighted error

$$\varepsilon_t = \min_{f,p,\theta} \sum_i w_i \left| h(x_i, f, p, \theta) - y_i \right|$$

  - Define $h_t(x) = h(x, f_t, p_t, \theta_t)$ where f_t ,p_t ,and θ_t are the minimizers of ε_t.
  - Update the weights:

$$w_{t+1,i} = w_{t,i} \beta_t^{1-e_i}$$

where $e_i = 0$ if example x_i is classified correctly, $e_i = 1$ otherwise, and $\beta_t = \frac{\varepsilon_t}{1-\varepsilon_t}$

- The final strong classifier is:

$$C(x) = \begin{cases} 1 & \sum_{t=1}^{T} \alpha_t h_t(x) \geq \frac{1}{2} \sum_{t=1}^{T} \alpha_t \\ 0 & otherwise \end{cases}$$

where $\alpha_t = \log \frac{1}{\beta_t}$

Cascade architecture [26][28] is a kind of degenerate decision tree which attempts to reject as many negatives as possible at earliest stage possible. A positive result from the first classifier triggers the evaluation of a second classifier and a positive result from the second classifier triggers the evaluation of a third classifier, and so on. However, a negative outcome at any point leads to be reject immediately. Figure 4-2 shows the schematic depiction of a cascade classifier.

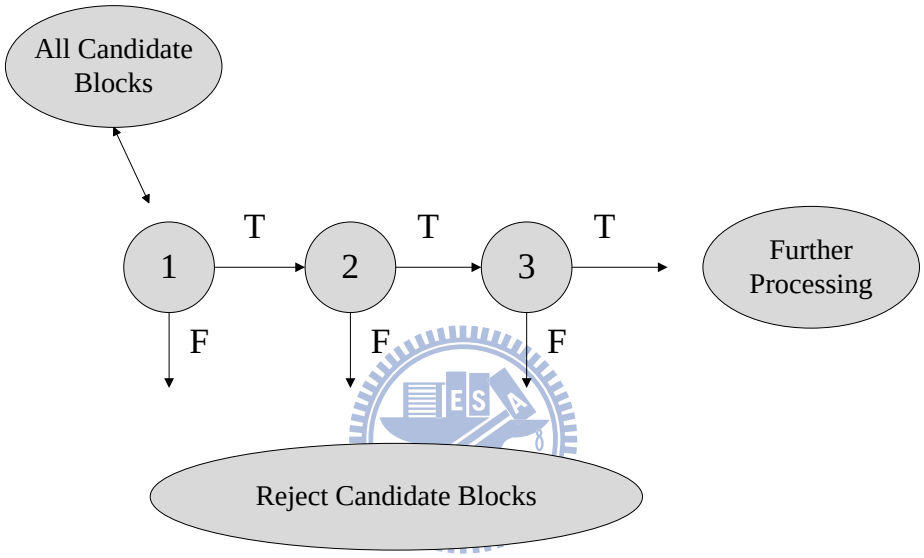

Fig. 4-2 Schematic depiction of a cascade classifier

The number of cascade stages and the size of each stage must be sufficient to achieve similar detection performance while minimizing computation. Given a trained cascade of classifiers, the false positive rate of the cascade

$$F = \prod_{i=1}^{K} f_i \tag{4.2}$$

where F is the false positive rate of the cascaded classifier, K is the number of classifiers, and f_i is the false positive rate of the ith classifier on the examples that get through to it.

The detection rate is

$$D = \prod_{i=1}^{K} d_i \tag{4.3}$$

where D is the detection rate of the cascaded classifier, K is the number of classifiers, and d_i is the detection rate of the ith classifier on the examples that get through to it.

The cascade design process is driven from a set of detection and performance goals. In most cases of classifiers training will achieve high detection rates and low false positive rates. Table 4-2 indicated the training algorithm for building a cascaded classifier.

Table 4-2 Training algorithm for building a cascaded detector.

- User selects values for f, the maximum acceptable false positive rate per layer and d, the minimum acceptable detection rate per layer.
- User slelets target overall false positive, $F_{target.}$
- P = set of positive examples
- N = set of negative examples
- $F_0 = 1.0$; $D_0 = 1.0$
- i = 0
- while $F_i > F_{target}$
  - $i \leftarrow i + 1$
  - $n_i = 0$; $F_i = F_{i-1}$
  - *while* $F_i > f \times F_{i-1}$
    - $n_i \leftarrow n_i + 1$
    - Use P and N to train a classifier with n_i features using AdaBoost
    - Evaluate current cascaded classifier on validation set to determine F_i and D_i
    - Decrease threshold for the ith classifier until the current cascaded classifier has a detection rate of at least d x D_{i-1} (this also affects F_i)
  - $N \leftarrow 0$
  - If $F_i > F_{target}$ then evaluate the current cascaded detector on the set of non-smoke images and put any false detections into the set N

A very simple framework is used to produce an effective classifier which is highly efficient. Researcher selects the maximum acceptable rate for f_i = 0.3 and the minimum acceptable rate for d_i = 0.9. Each layer of cascade is trained by AdaBoost [26] (as described in Table 4-1) with the number of features used being increased until the target detection and false positive rates are met for this level. The complete arrangement of local feature cascade classifier is shows in figure 4-3.

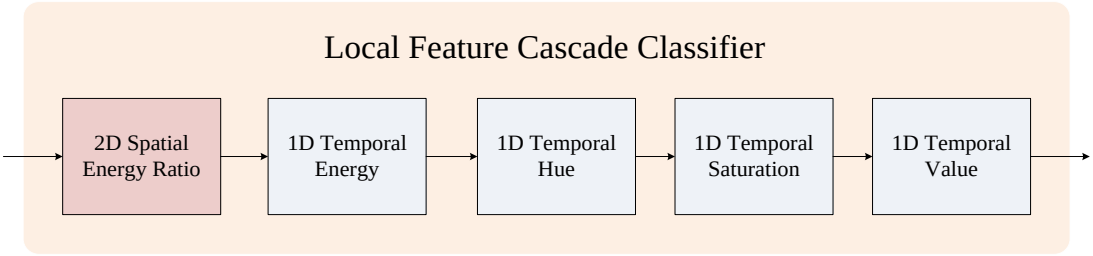

Fig. 4-3 Local feature cascade classifier

4.2 Global Feature Verification

Global feature verification is the final stage of proposed system. This is an important stage of the system because of the global feature verification has perfect discrimination ability with tough case such like big moving objects, light reflection with a big area and tree with vivid leafs, etc. Because all of these cases would meet the local features we proposed. To solve these problems, adding more local feature is inefficient. Combine each block in the same region to get whole region of the objects. At this time, we can analyze the region based features (global features) in each region. Therefore, block-based connected components were employed to combine each block in neighbor. In next section will introduce block-based connected components then will introduce the global feature verification method in our system: “Area ratio”, “Contour analysis” and “Region analysis”. Figure 4-4 illustrates the flow chart of global feature

verification.

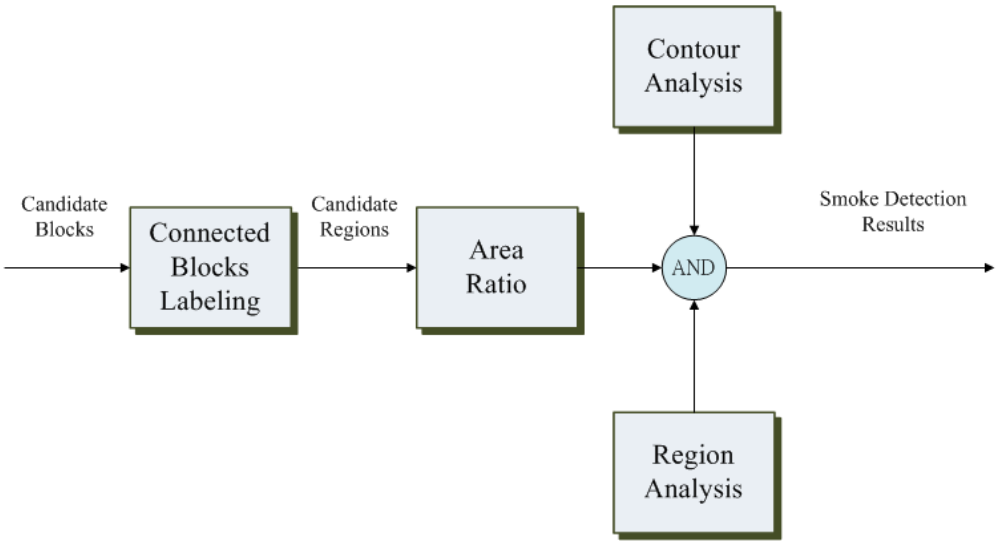

Fig. 4-4 Flow chart of global feature verification

4.2.1 Block-Based Connected Components

Connectivity between pixels is a fundamental concept that simplifies the definition of numerous digital image concepts, such as regions and boundaries. To establish whether these two pixels are connected, it is determined by their neighbors and finds their gray levels satisfy a specified criterion or similarity [27]. For instance, in binary image with values 0 and 1, two pixels maybe 4-neighbors, but they are said to be connected only if they have the same value.

Let V be the set of gray-level values used to define adjacency. In a binary image, V = {1} if we are referring to adjacency of pixels with value 1. We consider three types of adjacency/connectivity [27]:

1. 4-connectivity

Two pixels p and q with values from V are 4-connectivity if q is in the set N4(p).

2. 8-connectivity

Two pixels p and q with values from V are 8-connectivity if q is in the set N8(p).

3. m-connectivity

Two pixel p and q with values from V are m-connectivity if

(i) q is in N4(p), or

(ii) q is in ND(p) and the set N4(p) ∩ N4(q) has no pixels whose values are from V.

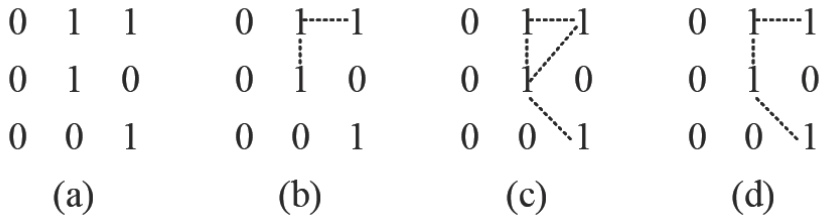

Fig. 4-5 (a) Arrangement of pixels (b) pixels that are 4-connectivity (c) pixels that are 8-connectivity (d) m-connectivity

Figure 4-5 (a) shows a binary image which uses to find the connectivity between every pixel. Figure 4-5 (b) shows the 4-connectivity, pixel p has 4-connectivity to its neighbor which in horizontal or vertical position and contain V= {1}. If pixel p has connectivity to neighbor pixel in horizontal, vertical or diagonal position, it will define as 8-connectivity. The last figure is m-connectivity is a modification of 8-connectivity introduced to eliminate the ambiguities that often arise when 8-connectivity is used. The three pixels at the top of Fig. 4-5 (c) show ambiguous of 8-connectivity, as indicated by the dashed lines. This ambiguity is removed by using m-connectivity, as shown in Fig. 4-5 (d).

Connected component works by scanning an image, pixel-by-pixel in order to identify connected pixel regions [31]. Its works on binary or gray-level images and different measures connectivity are possible. Choice of the connectivity is among 4, 8,

6, 10, 18, 26 connectivity which are 4 and 8-connectivity for 2-D connected component extraction and the others for 3D connected component extraction. The connected components labeling operator scans an image by moving a row along until it comes to a point p where denotes the pixel to be labeled at any stage in the scanning process for which V= {1}. When this constrain is satisfied, it examines the four neighbors of p which already been encountered in the scan. Based on this information, the labeling of p occurs as follows:

(i) If all four neighbors are 0, assign a new label to p, else

(ii) If only one neighbors has V={1}, assign its label to p, else

(iii) If one or more of the neighbors have V = {1}, assign one of the labels to p and make a note of the equivalence. For this case, we are labeling p with minimum label value.

Fig. 4-6 Connected components labeling

Once all groups have been determined, each pixel in same component will be labeled with same label. Figure 4-6 shows the results of connected components labeling. According to this concept, gird based connected components labeling was proposed. Each candidate block in the same moving object will be labeled with same label. Figure 4-7 shows a block based connected components labeling. Different colors stand for different components respectively.

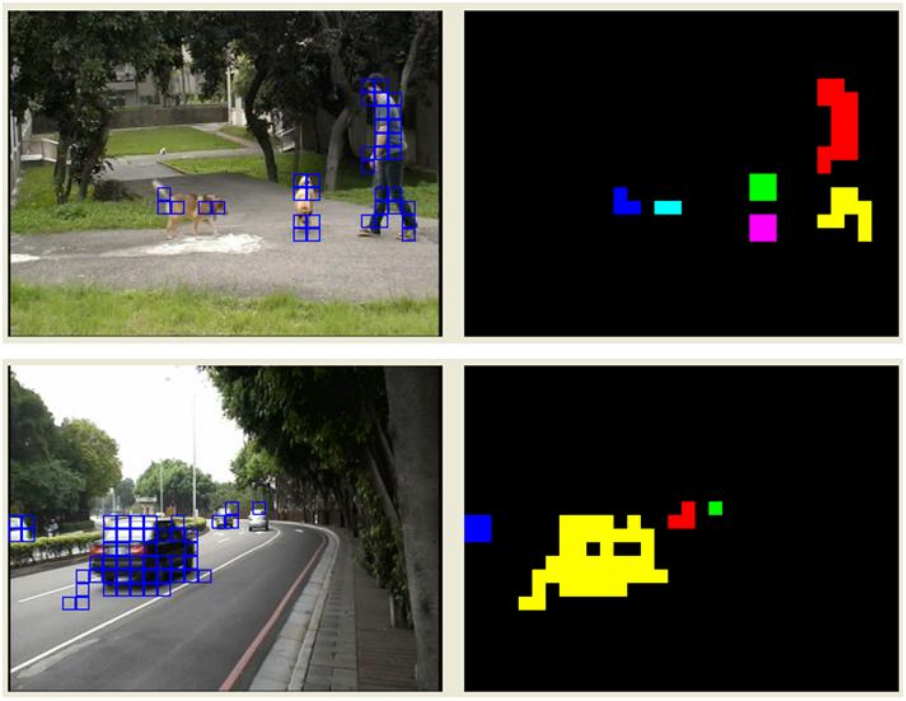

Fig. 4-7　Regard a block as a pixel unit

The presented system is an ensemble of different modules as depicted in Fig. 4-7. The main scope of this paper is the feature extraction and classification with respect to candidate block and candidate region of moving objects.

4.2.2　Area Ratio

When the ratio between the number of smoke blocks and the number of total blocks within a specific label is larger than a predefined value, in this study case, 0.25 is an experimental value of the ratio, all blocks in this label are painted “red” to represent smoke candidate regions and “green” to represent non-smoke regions as Fig. 4-8 shows. This verification can eliminate false detected candidate blocks inside ordinary moving objects and smoke regions.

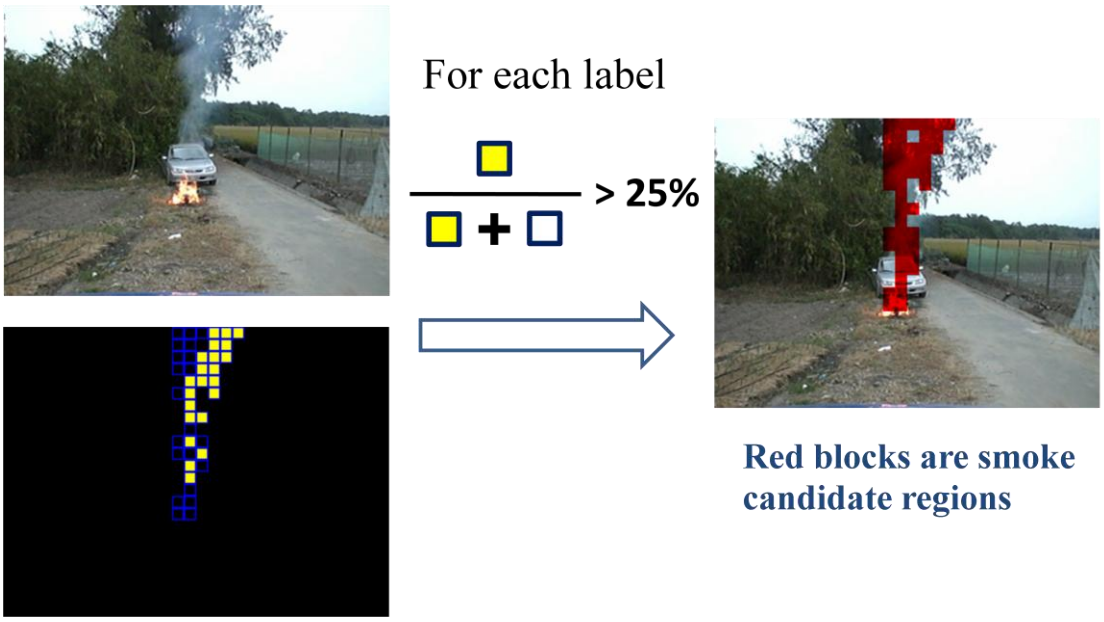

(a)

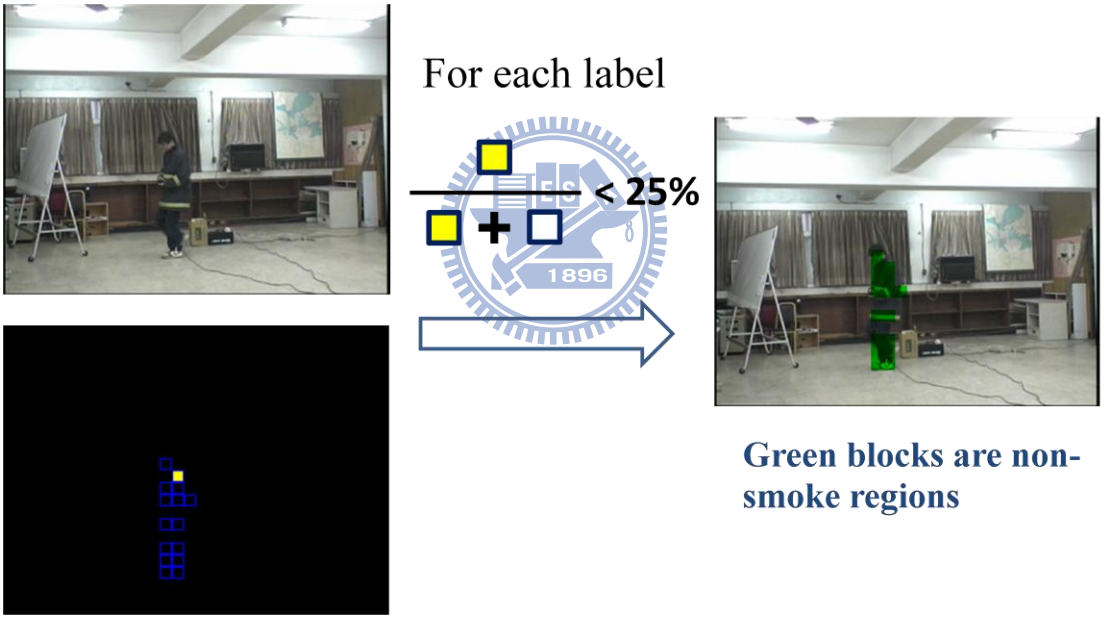

(b)

Fig. 4-8 Result of Connected blocks labeling. (a) The upper left picture is a sample frame with smoke objects and the lower left picture shows the smoke blocks are painted "yellow" and the non-smoke blocks are represented by "blue" blocks. The right picture is the result of connected blocks labeling. All blocks in this label are painted "red" to represent smoke candidate regions. (b) The upper left picture is a sample frame with ordinary moving objects and the lower left picture shows the smoke blocks are painted

“yellow” and the non-smoke blocks are represented by “blue” blocks. The right picture is the result of connected blocks labeling. All blocks in this label are painted “green” to represent non-smoke regions

4.2.3 Contour Analysis

Sometimes the camera is set too close to the ground in video surveillance systems and the infrared camera in dark space would cause the color configuration changing monochromatically. In this situation, the energy ratio would change smoothly because of the objects are too close to the camera and the features relative to color configuration would not active entirely. Contour analysis was proposed to overcome this kind of false positive. Figure 4-9 (c) shows the contour of candidate regions.

(a) (b) (c)

Fig. 4-9 Results of contour extraction. (a) Sample frame from the test sequence (b) Candidate region of the moving objects (c) Contour of the candidate region

To reduce the computation cost on contour extraction. An approximate method to extract the contour of the region was employed. Four-neighbors including up, down, left and right of the blocks just like four-connectivity analysis. If there is a non-candidate block to its four neighbors then it will be determined as a contour blocks on this region. Otherwise, it will be regarded as the interior blocks of this region. In general, smoke contour has a high-transparent property and blurs edges and textures in the background. High-frequency information becomes much more invisible. However,

it still reveals the background information. On the contrary, the ordinary solid moving objects do not have the transparent property, so the background information will be covered by the moving objects. Energy ratio between foreground and background will severe change abruptly. Energy ratio between foreground and background is calculated for each candidate region：

$$\omega_1 = \frac{\sum_{k \in C_i} \alpha(B_k, t)}{blocks\ number\ of\ C_i} \tag{4.4}$$

where C_i is the *i*th candidate region's contour of the scene, $\alpha(B_k,t)$ is the *k*th candidate block's wavelet ratio of the scene. Ordinary solid moving objects produce a great quantity of energy changing. Smoke has a smooth variation in energy ratio value and produces a few of changing in the average wavelet energy ratio on contour. The likelihood of the candidate region to be a smoke region is the value of ω_1 in the predefined value range. This value range is trained by 8798 positive (smoke) training samples. Fig. 4-10 shows the diffusion of car lights and reflects on the road and makes a lot of noise. In such situation, the moving foreground caused by light reflection will blurs the texture and edges in the background. Color configuration analysis doesn't work at night. So, many regions will be miscalculation as smoke regions. Contour analysis plays a significant role to overcome the miscalculation in such situation.

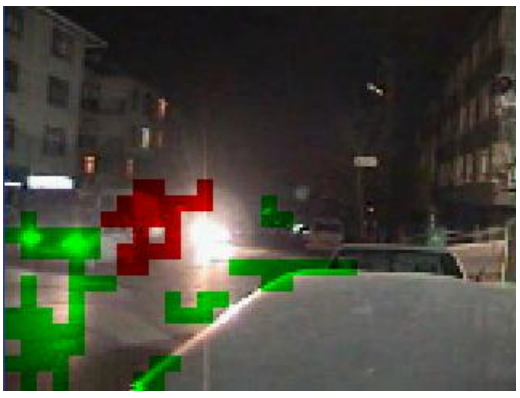

(a)

(c)

(b) (d)

Fig. 4-10 Car lights diffusion and reflects on the road. (a) Smoke detection result may determine the region as a smoke candidate region before contour analysis. (b) Shows the contour of the moving object and different color means the different region. (c) Smoke detection result determines the region as a non-smoke region after contour analysis. (d) Contour analysis rejects this non-smoke candidate region and represented by “black” blocks.

4.2.4 Region Analysis

Global feature only according to the energy ratio between the foreground and the background is not strong enough. Sometimes both of the foreground energy and the background energy are extremely high and have similar value. Thus, it will cause the energy ratio between foreground and background nears to the property to smoke. In such case, the energy ratio caused by waving leaves might similar to the energy ratio caused by smoke through the scene. Figure 4-11 illustrates the false positive cause by waving leaves.

Fig. 4-11 False alarms caused by waving leaves

This approach can deal properly with the false positive causing by complex moving foreground, especially in leaves waving in the wind and man squirm. The average of foreground energy is calculated for each candidate region：

$$\omega_2 = \frac{\sum_{k \in R_i} E(B_k, I_t)}{blocks\ number\ of\ R_i} \tag{4.5}$$

where R_i is the ith candidate region's interior blocks in the scene, $E(B_k,t)$ is the kth candidate block's wavelet energy in the scene. Complex solid moving objects produce a great quantity of energy changing. Smoke has a smooth variation in energy value and produces a few of changing in the average wavelet energy. The likelihood of the candidate region to be a smoke region is the value of ω_2 in the predefined value range. This value range is trained by 9334 positive (smoke) training samples. Fig. 4-12 shows the output after region analysis in each candidate region.

Fig. 4-12 Output after region analysis

This approach can properly deal with continuous waving leaves or man squirm. Combined the “Area Ratio”, “Contour Analysis” and “Region Analysis” to obtain our global feature verification, the desired output is coming out from the verification stage. The global feature verification eliminated miscalculations or transient noise and enhancement the system stability.

Chapter 5

Experimental Results

In this chapter, several results of smoke detection will be presented. Our algorithm was implemented on PC with Intel Core2 Quad 2.4GHz and 2GB RAM. Borland C++ Builder is our complier and operated on Windows XP. There are many different kinds of compressed format AVI testing inputs and DVD video data acquired by USB video capture. Some of testing videos are downloaded from the webpage (http://www.openvisor.org [29] and http://signal.ee.bilkent.edu.tr/VisiFire/index.html [30]) and the other testing films are made by other researchers in our lab. Each video sequence has a resolution of 320×240.

In section 5.1, we will show the experimental results of the proposed algorithm on different scenes. Besides, accuracy rate and comparison between features are demonstrated in section 5.2. A brief discussion of our proposed algorithm will be presented in section 5.3.

5.1 Experimental Results of Smoke Detection

The testing videos in this study contain various conditions, including indoor, outdoor and sunlight variation each containing smoke events, pedestrians, bicycles, motorcycle, tourist coaches, trailers, waving leaves, etc. All of the testing videos are list in appendix, including 39 smoke videos and 42 non-smoke videos. All videos contain 63000 positive samples (frames with smoke objects) and 113269 negative samples (frames with only non-smoke objects). “Red” blocks represent smoke regions and “Green” blocks represent non-smoke regions. The columns of left side contain

original video sequence and the columns of right side contain detection results of the proposed algorithm.

Figure 5-1 illustrates the outdoor environments situation. No wind exhibits in Fig. 5-1(a), but the wind is blowing hard in Fig. 5-1(b)(c)(d) and smoke strongly floats in the air. The features wouldn't be affected by the external environments and smoke regions can be detected correctly.

(a)

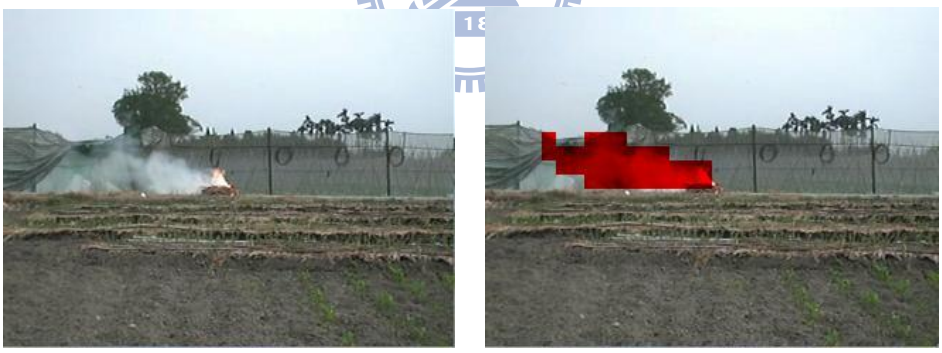

(b)

(c)

(d)

Fig. 5-1　Outdoor environments

Figure 5-2 illustrates the outdoor environments with pedestrians. Smoke regions can be detected correctly even when people walk around.

(a)

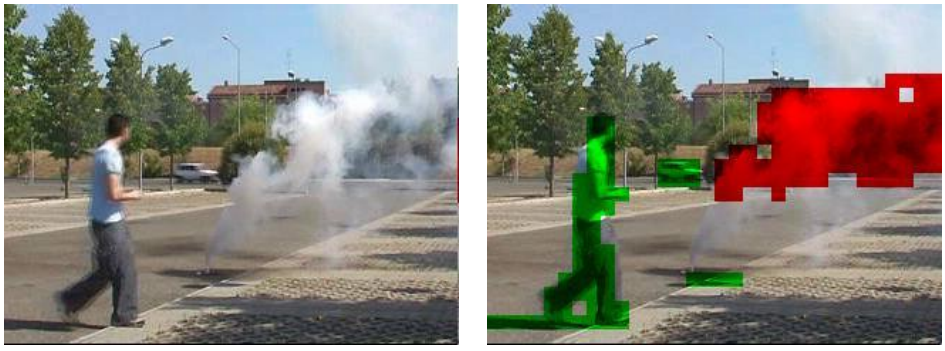

(b)

(c)

Fig. 5-2　Outdoor environments with people

Figure 5-3 illustrates the outdoor environments with vehicles. Smoke regions can be detected correctly even when vehicles go through the scene. There are cars, motorcycles and trucks, etc in our testing data.

(a) Cars

(b) Motorcycles

Fig. 5-3　Outdoor environments with vehicles

Figure 5-4 illustrates the indoor environments situation. Smoke regions can be detected correctly. Smoke regions can be detected correctly even when people walk around.

(a)

(b)

(c)

Fig. 5-4 Indoor environments

The following discusses the testing results of real traffic situations in tunnels and fire accident in tunnels with heavy smoke. Figure 5-5(a)(b)(c) illustrate the tunnel

environments with smoke objects. The proposed algorithm can detect smoke precisely and issue alarms in time.

(a)

(b)

(c)

Fig. 5-5 Smoke objects in tunnels

Figure 5-6(a)(b)(c)(d) show different vehicles presence in a tunnel and they don't activate alarm even the luminance changing in suddenly including car lights, shadow and sunlight reflection. Figure 5-6(e)(f) show cars in the tunnels at night. Figure

5-6(g)(h) show cars in a tunnel in day time. Both situations don’t produce false alarms.

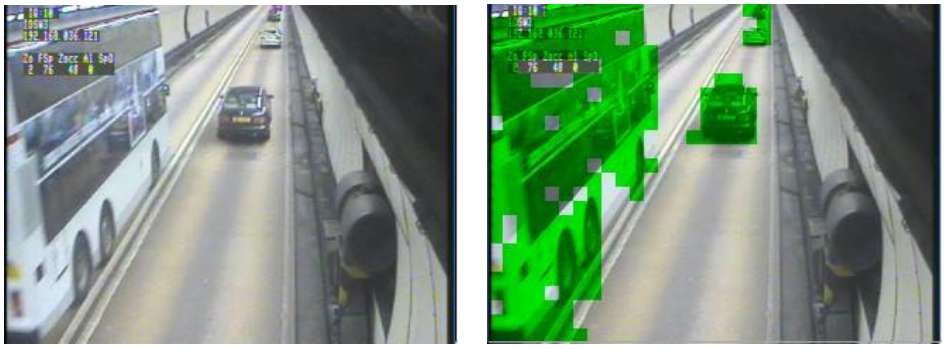

(a) Real traffic situations in a tunnel

(b) Real traffic situations in a tunnel

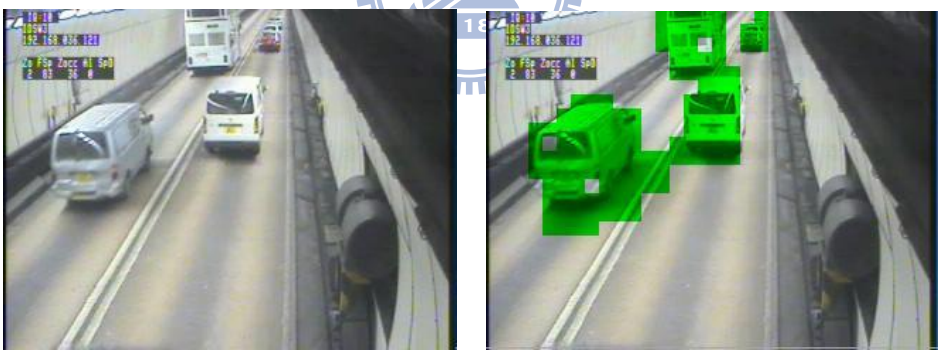

(c) Real traffic situations in a tunnel

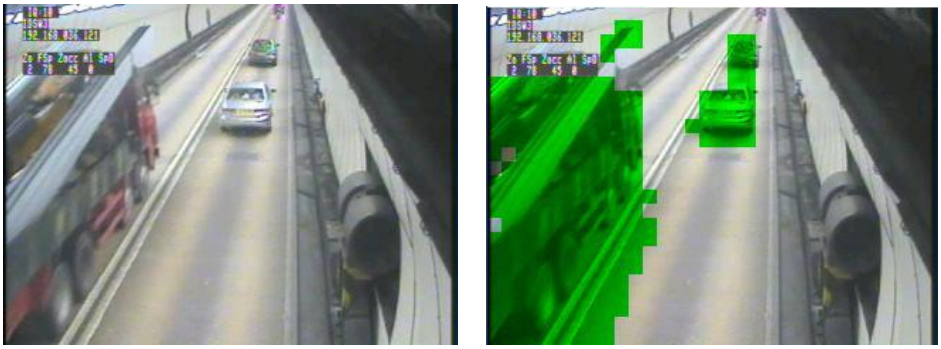

(d) Real traffic situations in a tunnel

(e) Real traffic situations in a tunnel

(f) Real traffic situations in a tunnel

(g) Real traffic situations in a tunnel

(h) Real traffic situations in a tunnel

Fig. 5-6 Tunnel environments

Several traffic conditions in these data include traffic jams and huge tourist coaches and trucks. The total length of the testing data is four hours and smoke regions are detected correctly.

5.2 Accuracy Discussion

This study proposes a frame-based and video-based criterion to quantitatively evaluate video smoke detection system. Data in Table 5-1 show the evaluations of each local and global feature testing result. The reaction time is obtained by the ratio between frames to detect and frames per second. The false positive rate is calculated as follow：

$$\text{False Alarm Rate} = \frac{N_{\text{false detected}}}{N_{\text{non-smoke}}} \times 100\% \tag{5.2}$$

In local features classification, 2-D spatial wavelet analysis can successfully extract candidate blocks with energy drop. However, pedestrians wearing flat clothing or long vehicles with flat roofs also produce energy drop. To overcome this drawback, 1-D temporal wavelet analysis be proposed to express the gradual change of the energy ratio of smoke regions. This approach can adequately simulate the temporal characteristic of smoke. In some real cases, background model and foreground objects are so flat that there is no apparent high frequency information. It is difficult to separate smoke from non-smoke regions. In this situation 1-D temporal color configuration analysis due to further describe the smoke's behavior. The local features experimental results are described in Table 5-1.

Table 5-1 Local features experimental results based on single frame

Local Features	False alarm rate
2-D Energy Ratio Analysis	16.23%
1-D Energy Analysis	24.99%
1-D Hue Analysis	40.45%
1-D Saturation Analysis	28.94%
1-D Value Analysis	42.48%

In global features verification, Area ratio analysis combines the smoke blocks and non-smoke blocks from the results of cascade classifier. An experiential threshold would distinguish smoke regions from non-smoke regions approximately. In some tough cases such like waving leaves, pedestrians wearing flat clothing in a lightless room, etc. It is still difficult to separate smoke from non-smoke regions certainly. Contour analysis and region analysis further refuses the false positive rate with low true positive rate decrease. The global features experimental results are described in Table 5-2.

Table 5-2 Global features experimental results based on single frame

Global Features	False alarm rate
Cascade + Area Ratio	**0.19%**
Contour Analysis	37.26%
Region Analysis	38.76%

In Table 5-3, the cascade classifier learns the optimal combination relationship among the five features and gains the low false alarm rate, which is 0.19%. Furthermore, the results of combining the local features with the global features shows that, the global feature verification further decreases the false alarm rate from 0.19% to 0.024%, while slightly decrease the detection rate. Overall system provides a precise detection rate and reaches 97.2% in total testing videos.

Table 5-3 Experimental results with combine the local features and global features

	False alarm rate	Video-based detection rate
Cascade + Area Ratio	0.19%	-
Total	**0.024%**	**97.2%**

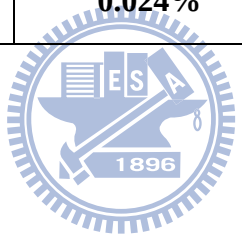

5.3 Comparison

The analysis of experiments implementing the proposed process derived in previous sections is presented in this section. The testing films are separated in four sets named UE-Lab, UE-Tunnel, Cetin and Visor, and are listed in Table 5-4 to Table 5-7 respectively. Including 32 smoke videos and 14 non-smoke videos over 50000 smoke frames and 54000 non-smoke frames. Two kinds of comparative manners are proposed in this study case. Video-based comparison can let us know the system's stability in different environments. Frame-based comparison can let us know how the system performed in each environment. A series of discussions will be presented.

Table 5-4 Properties of the test video in UE-Lab

Movie List	Description
Farm	Fast smoke with a pedestrian
Side Road	Light smoke with pedestrians, bicycles, cars and waving leaves
Left House	Light smoke with pedestrians, waving leaves
Front House	Light smoke with pedestrians, truck, cars and waving leaves
White Car	Light smoke with a pedestrian
people_near_black	Near smoke in a room with a pedestrian
smoke_near	smoke in a room
raw_highway1	Fast cars on the highway with dark shadow
raw_highway2	Fast cars on the highway with shadow
B1001	Pedestrians pass through the automatic door
Lab001	Pedestrians walk around in the lab
Lab003	Pedestrians walk around in the lab

Table 5-5 Properties of the test video in UE-Tunnel

Movie List	Description
VTS_07_1	Light smoke in tunnel with pedestrians
TunnelSmoke	Dark smoke in tunnel with pedestrians
隧道1	Cars in tunnel
隧道2	Cars in tunnel in day time
隧道1D	Cars in tunnel at night
隧道1N	Cars in tunnel
隧道2D	Cars in tunnel in day time
隧道2N	Cars in tunnel at night
TunnelTruck	A trailer tows away a truck with pedestrians

Table 5-6 Properties of the test video in Cetin

Movie List	Description
sBehindtheFence	Far smoke behind the fence
sBtFence2	Near smoke behind the fence
sEmptyR1	Spring smoke with sunlight reflections
sEmptyR2.	Spring smoke with sunlight reflections
ShorterIsyamNight	Smoke in a room
sMoky	Light smoke in the yard
sParkingLot	Smoke in a parking lot
sWasteBasket	Fast smoke near to a wastebasket
sWindow	Smoke in the yard with a pedestrians
CarLights1	Cars with reflective light
CarLights2	Cars with reflective light

Table 5-7 Properties of the test video in Visor

Movie List	Description
visor_1196179837385_movie11_viper	Pedestrians walk through smoke
visor_1196343040120_movie12_viper	Light smoke with pedestrians and cars
visor_1196343142698_movie13_viper	Dark smoke with pedestrians and cars
visor_1196343179807_movie14_viper	Pedestrians walk through smoke
visor_1197283980290_10_hangar	Smoke in a hangar with a pedestrian
visor_1197283983165_01_ballistic	Outdoor explosion
visor_1197283985149_02_explosion	Outdoor explosion
visor_1197283985415_03_burnout_contest	Smoke in a parking lot with pedestrians
visor_1197283990821_04_fumogeno1	Light smoke with pedestrians and cars
visor_1197284001212_05_fumogeno2	Dark smoke with pedestrians and cars
visor_1197284006306_06_fumogeno3	Pedestrians walk through smoke
visor_1197284015696_07_fumogeno4	Light smoke with pedestrians and a car
visor_1197284021149_08_fumogeno5	Light smoke with pedestrians
visor_1197284028899_09_fumogeno6	Light smoke with a pedestrian and a car

In this study, researchers used these four testing sets to compare the system proposed in [7][23] with the system proposed by us. First testing set includes many kinds of indoor and outdoor environments. There have seven smoke videos and five non-smoke videos in this testing set. In this testing set, the system proposed by us detects all the smoke events and has a shortest reaction time of the three systems. Three systems active alarm in non-smoke videos at least one times. Because of the videos are make by infrared camera and in a lightness room. So, the video quality will increase the possibility of false alarm. Table 5-8 and Table 5-9 depicted the testing results in UE-Lab testing set. Totally, includes 20975 smoke frames and 14923 non-smoke frames in this testing set.

Table 5-8 Video-based comparative results with UE-Lab

	# Detected smoke videos	**# False alarmed videos**
This study	**7**	**1**
C.Y. Lee and C.T. Lin	7	3
Töreyin, et. al	2	3

Table 5-9 Frame-based comparative results with UE-Lab

	False alarm rate	**Reaction time (sec)**
This study	**0.1%**	**1.21**
C.Y. Lee and C.T. Lin	0.48%	1.57
Töreyin, et. al	0.93%	1.77

Two smoke videos and seven non-smoke videos are shot in the tunnels. Because the method in [7] only utilized the concept of wavelet energy, which calculates the smooth degree of the moving objects. However, this testing set contains lots of vehicles pass through in tunnel. Fake alarms are activated and result in high false alarm rate.

This testing includes 5583 smoke frames and 28781 non-smoke frames.

Table 5-10 Video-based comparative results with UE-Tunnel

	# Detected smoke videos	**# False alarmed videos**
This study	**2**	**2**
C.Y. Lee and C.T. Lin	2	3
Töreyin, et. al	2	7

Table 5-11 Frame-based comparative results with UE-Tunnel

	False alarm rate	**Reaction time (sec)**
This study	**0.1%**	**1.13**
C.Y. Lee and C.T. Lin	1.5%	1.08
Töreyin, et. al	7%	1.52

This testing set includes 9 smoke videos and 2 non-smoke videos and we downloaded from the webpage (http://signal.ee.bilkent.edu.tr/VisiFire/index.html [30]). The proposed system miss one smoke video in this testing set, so does the system proposed by [23]. Both of our systems need to construct background at the system beginning. However, most parts of testing videos in this testing set, smoke strongly floats in the air in beginning. But, our systems have a better reaction time in this testing set.

Table 5-12 Video-based comparative results with Cetin

	# Detected smoke videos	**# False alarmed videos**
This study	**8***	**0**
C.Y. Lee and C.T. Lin	8*	2
Töreyin, et. al	9	0

Table 5-13 Frame-based comparative results with Cetin

	False alarm rate	**Reaction time (sec)**
This study	**0%**	**7.86**
C.Y. Lee and C.T. Lin	3.26%	6.71
Töreyin, et. al	0%	9.57

The fourth testing set is downloaded from the webpage (http://www.openvisor.org [29]) and includes 14 smoke videos. All of videos in this testing set are shot in open space. The proposed algorithm detects smoke precisely and issues alarms in time. The other proposed systems miss at least one smoke video in this testing set.

Table 5-14 Video-based comparative results with Visor

	# Detected smoke videos	**# False alarmed videos**
This study	**14**	**0**
C.Y. Lee and C.T. Lin	13	0
Töreyin, et. al	11	4

Table 5-15 Frame-based comparative results with Visor

	False alarm rate	**Reaction time (sec)**
This study	**0%**	**3.74**
C.Y. Lee and C.T. Lin	0%	1.64
Töreyin, et. al	2.65%	9.3

The comparative results show that the proposed system can well detect smoke with low false alarm rate within a short reaction time in various environments.

Chapter 6

Conclusions and Future Work

It is inefficient to track or analyze the target using object-based method. Block-based technique provides a better way to solve this problem; 1-D Temporal analysis is introduced to express gradual changes of energy and chromatic configuration in smoke regions and the features would not be affected by the external environment; Boosting cascade algorithm improves the system efficiency and optimizes the feature combination. Global features are proposed to overcome the shortcoming of local features and enhance the system stability.

Most of other's algorithms are only seeking higher detection rate. It does not provide enough information on how accurate the system might be. When considering accuracy of smoke detection, people care more about how to decrease the false alarm rate and detect smoke events quickly, rather than just increase the detection rate. Here the false alarm rate of the proposed system is significantly lower than other's and the reaction time is extremely short. This system can also locate the smoke regions correctly even when both smoke and non-smoke objects exist in the same frame due to block processing while other systems only detect whether there is smoke existing in the whole video or the single frame.

The proposed algorithm can be operated well in variant environment. However, to further improve the performance of our system, some enhancements or trials can be made in the future. Firstly, it would cause false alarm when GMM background update strongly. Especially, system would activate alarm when the object stayed for a long time and then it leaved. In such situation, background updating broke the constructed background thoroughly. Because the decrease in energy and the similarity in chromatic

configuration. To avoid false alarm in background updating, researchers proposed to use the background before strong updating and wait until the background constructed completely. Secondly, the infrared camera in dark room would cause the color configuration changing monochromatically. In this situation, the features relative to color configuration would not active entirely. Therefore, if these problems can be solved, this algorithm will be more reliable.

This paper demonstrates a robust and efficient system for smoke detection, and it involves the global and local features analysis for each candidate block and the boost and cascade architecture. Experimental results show the opportunity of the real-time operation of surveillance systems and advanced applications. The false alarm rate of the proposed system is lower than that of the state of art. The proposed algorithm has low computation load and has been implemented on embedded system.

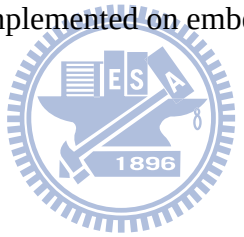

References

[1] Vicente, P. Guillemant, “An image processing Technique for automatically detecting forest fire,” *International Journal of Thermal Sciences*, vol. 41, Issue 12, pp. 1113-1120, December 2002.

[2] B. Toreyin, Y. Dedeoglu, A. Cetin, “Wavelet based real-time smoke detection in video,” in *Proceedings of the 13th European Signal Processing Conference, EUSIPCO’05*, Antalya, Turkey, 2005, pp. 4–8.

[3] Kopilovic, B. Vagvolgyi and T. Sziranyi, "Application of panoramic annular lens for motion analysis tasks: surveillance and smoke detection," *In Proc. ICPR*, Barcelona, 2000.

[4] Feiniu Yuan, "A fast accumulative motion orientation model based on integral image for video smoke detection," *Pattern Recognition Letters*, vol. 29, pp.925-932, May 2008.

[5] Thou-Ho Chen, Yen-Hui Yin, Shi-Feng Huang and Yan-Ting Ye, "The smoke detection for early fire-alarming system base on video processing," in *Proceeding of the 2006 international Conference in intelligent information Hiding and Multimedia Signal Processing* , IIH-MSP'06.

[6] Jing Yang, Feng Chen and Weidong Zhang, "Visual-based smoke detection using support vector machine," *Fourth International Conference on Natural Computation*, vol. 4, pp.301-305, ICNC '08, 2008.

[7] Töreyin, B.U., Dedeoğlu, Y., Çetin, A.E., ”Contour based smoke detection in video using wavelets,” in *Proceedings of 14th European Signal Processing Conference, EUSIPCO’06*, Florance, Italy, 2006

[8] P. Guillemant and J. Vicente, “Real-time identification of smoke images by clustering motions on a fractal curve with a temporal embedding method,” *Optical Engineering*, vol. 40, no. 4, pp. 554–563, 2001.

[9] N. Fujiwara and K. Terada, “Extraction of a smoke region using fractal coding,” *IEEE International Symposium on Communications and Information Technology, 2004*, ISCIT 2004, vol. 2, 26-29 Oct. 2004, pp. 659 - 662.

[10] Z. Xiong, R. Caballero, H. Wang, A.M. Finn, M.A. Lelic, P.Y. Peng, “Video-based smoke detection: possibilities, techniques, and challenges,” in: *IFPA, Fire Suppression and Detection Research and Applications—A Technical Working Conference, SUPDET*, 2007.

[11] Chao-Ching Ho, ”Machine vision-based real-time early flame and smoke detection,” *Measurement Science and Technology*, vol. 20, no. 4, March 2009.

[12] Capitan. J, Mantecon. D, Soriano. P and Ollero. A, "Autonomous perception techniques for urban and industrial fire scenarios," *IEEE International Workshop on Safety, Security and Rescue Robotics*, pp.1-6, SSRR 2007.

[13] Chan-Yun Yang, Wei-Wen Tseng, Jr-Syu Yang, "Reducing false alarm of video-based smoke detection by support vector machine," *ISI Workshops* 2008, pp. 102-113.

[14] S. Calderara, P. Piccinini, R. Cucchiara, "Smoke detection in video surveillance: a MoG model in the wavelet domain", *Lecture Notes in Computer Science*, no. 5008, pp. 119-130, 2008

[15] A. E. Cetin and R. Ansari, "Signal recovery from wavelet transform maxima," *IEEE Trans. on Signal Proc.*, vol.42, pp.194-196, 1994.

[16] Piccinini. P, Calderara. S and Cucchiara. R, "Reliable smoke detection in the domains of image energy and color," in: *Proceedings of 15th IEEE International Conference on Image Processing*, pp.1376-1379, ICIP 2008.

[17] C. L. Lai, J. C. Yang, and Y. H. Chen. "A real time video processing based surveillance system for early fire and flood detection", in: *Proceedings of 2007 IEEE Instrumentation and Measurement Technology Conference*, 1-6, May 2007.

[18] H. Maruta, Y. Kato, A. Nakamura, F. Kurokawa, "Smoke detection in open areas using its texture features and time series properties, " in: *Proceedings of 2009 IEEE International Symposium on Industrial Electronics*, pp. 1904-8, Seoul, South Korea, 5-8 July 2009.

[19] Yu Chunyu, Zhang Yongming, Fang Jun, Wang Jinjun, "Texture Analysis of Smoke for Real-Time Fire Detection," in: *Proceedings of Second International Workshop on Computer Science and Engineering*, vol. 2, pp.511-515, 2009.

[20] Z. Xu, J. Xu, "Automatic fire smoke detection based on image visual features, " in: *Proceedings of International Conference on Computational Intelligence and Security Workshops*, CISW 2007, pp. 316–319.

[21] J. Capitan, D. Mantecon, P. Soriano, and A. Ollero, "Autonomous perception techniques for urban and industrial fire scenarios," in: *Proceedings of IEEE International Workshop on Safety, Security, and Rescue Robotics (SSRR)*, Rome, Italy, September 2007, pp. 1-6.

[22] J. Gubbim, S. Marusica, and M. Palaniswamia, "Smoke detection in video using wavelets and support vector machines", *Fire Safety Journal*, vol. 44, Issue 8, pp. 1110-1115, November 2009.

[23] Chen-Yu Lee, Chin-Teng Lin, Chao-Ting Hong, "Spatio-temporal analysis in smoke detection", *Signal and Image Processing Applications (ICSIPA), 2009 IEEE International Conference on*, vol., no., pp.80-83, 18-19 Nov. 2009.

[24] Dong-Keun Kim and Yuan-Fang Wang, "Smoke Detection in Video", CSIE 2009, LA.

[25] Stauffer. C, Grimson. W.E.L, "Adaptive background mixture models for real-time tracking", *IEEE Computer Society Conference on Computer Vision and Pattern Recognition*, vol. 2, June 1999.

[26] Viola Paul and J. Jones. Michael, "Robust Real-Time Face Detection", *International Journal of Computer Vision 57(2)*, 137-154, 2004

[27] R. C. Gonzales and R. C. Woods, Digital image processing, Prentice Hall, 2002.

[28] Luo-Wei Tsai, Jun-Wei Hsieh, Kuo-Chin Fan, "Vehicle Detection Using Normalized Color and Edge Map", *IEEE Transactions on image processing*, vol. 16, no. 3, March 2007.

[29] http://www.openvisor.org

[30] http://signal.ee.bilkent.edu.tr/VisiFire/index.html

[31] http://homepages.inf.ed.ac.uk/rbf/HIPR2/label.htm

Appendix

39 Smoke testing videos

Number	File Name	Descriptions
1	Farm	Fast smoke with a pedestrian
2	Side Road	Light smoke with pedestrians, bicycles, cars and waving leaves
3	Left House	Light smoke with pedestrians, waving leaves
4	Front House	Light smoke with pedestrians, truck, cars and waving leaves
5	White Car	Light smoke with a pedestrian
6	People_far_black.	Far smoke in a room with a pedestrian
7	People_far_white	Far smoke in a room with a pedestrian
8	people_near_black	Near smoke in a room with a pedestrian
9	people_near_white	Near smoke in a room with a pedestrian
10	smoke001	Fast and light Smoke in a room
11	smoke002	Fast and light Smoke in a room
12	smoke_far	Smoke in a room
13	smoke_near	Smoke in a room
14	smoke_side	Smoke in a room
15	VTS_07_1	Light smoke in tunnel with pedestrians
16	tunnel	Dark smoke in tunnel with pedestrians
17	sBehindtheFence	Far smoke behind the fence
18	sBtFence2	Near smoke behind the fence
19	sEmptyR1	Spring smoke with sunlight reflections
20	sEmptyR2.	Spring smoke with sunlight reflections
21	ShorterIsyamNight	Smoke in a room
22	sMoky	Light smoke in the yard
23	sParkingLot	Smoke in a parking lot
24	sWasteBasket	Fast smoke near to a wastebasket
25	sWindow	Smoke in the yard with a pedestrians
26	visor_1196179837385_movie11_viper	Pedestrians walk through smoke
27	visor_1196343040120_movie12_viper	Light smoke with pedestrians and cars
28	visor_1196343142698_movie13_viper	Dark smoke with pedestrians and cars
29	visor_1196343179807_movie	Pedestrians walk through smoke

	14_viper	
30	visor_1197283980290_10_hangar	Smoke in a hangar with a pedestrian
31	visor_1197283983165_01_ballistic	Outdoor explosion
32	visor_1197283985149_02_explosion	Outdoor explosion
33	visor_1197283985415_03_burnout_contest	Smoke in a parking lot with pedestrians
34	visor_1197283990821_04_fumogeno1	Light smoke with pedestrians and cars
35	visor_1197284001212_05_fumogeno2	Dark smoke with pedestrians and cars
36	visor_1197284006306_06_fumogeno3	Pedestrians walk through smoke
37	visor_1197284015696_07_fumogeno4	Light smoke with pedestrians and a car
38	visor_1197284021149_08_fumogeno5	Light smoke with pedestrians
39	visor_1197284028899_09_fumogeno6	Light smoke with a pedestrian and a car

42 Non-smoke testing videos

Number	File Name	Descriptions
1	0316001	Pedestrians walk in the campus
2	0316002	At side road and a pedestrian walk on the sidewalk
3	0316003	At side road and a pedestrian walk on the sidewalk
4	0316004	Pedestrian plays with dogs in the campus
5	0316005	Pedestrians walk in the campus
6	0316006	Pedestrians walk in the campus
7	B1001	Pedestrians pass through the automatic door
8	Lab001	Pedestrians walk around in the lab
9	Lab002	Pedestrians walk around in the lab
10	Lab003	Pedestrians walk around in the lightless lab
11	Lab003-1	Pedestrians walk around in the lightless lab
12	Lab004	Pedestrians walk around in the lab
13	Lab005	Pedestrians walk around in the lab
14	Lab006	Pedestrians walk around in the lab
15	LabOut001	Pedestrians walk in the campus
16	video_out	Pedestrians walk in the campus
17	muti005	Pedestrians walk in the campus
18	test001	Pedestrians walk in the campus
19	zHB000	Pedestrians walk in the campus
20	zHB001	Pedestrians walk in the campus
21	zHB002	Pedestrians walk in the campus
22	zHB003	Pedestrians walk in the campus
23	zHB004	Pedestrians walk in the campus
24	zHB005	Pedestrians walk in the campus
25	Produce_4	Cars in tunnel
26	隧道1	Cars in tunnel
27	隧道1D	Cars in tunnel in day time
28	隧道1N	Cars in tunnel at night
29	隧道2	Cars in tunnel
30	隧道2D	Cars in tunnel in day time
31	隧道2N	Cars in tunnel at night
32	Tunneltruck	A trailer tows away a truck with pedestrians
33	LightShadow_0	Fast cars on the highway with shadow
34	LightShadow_1	Fast cars on the highway with shadow

35	raw_highway1	Fast cars on the highway with dark shadow
36	raw_highway2	Fast cars on the highway with shadow
37	CarLights1	Cars with reflective light
38	CarLights2	Cars with reflective light
39	raw2	Fast cars on the highway with dark shadow
40	埔里隧道+陽光灑進	Cars in tunnel's entrance with sunlight variations
41	國姓一號隧道+逆行+施工車	Cars in tunnel's entrance with sunlight variations
42	國姓一號隧道lag	Cars in tunnel's exit with sunlight variations

Smoke detection results of UE-Lab (7 smoke videos and 5 non-smoke videos) testing set.

Video Info.			C.Y. Lee and C.T. Lin (SVD V1.0)		This study (SVD V2.0)		Töreyin, et. al	
Movie List	Frame Number	Smoke Frame Number	Frame To Detect	False alarm rate	Frame To Detect	False alarm rate	Frame To Detect	False alarm rate
Farm	5334	4410	31	0.0%	34	0.0%	13	0.0%
Side Road	4181	3561	20	0.0%	15	0.0%	82	0.0%
Left House	6467	3481	87	0.0%	48	0.0%	95	0.0%
Front House	4591	2764	60	0.0%	40	0.0%	56	0.0%
White Car	3303	1652	35	0.0%	27	0.0%	20	0.0%
people_near_black	2608	2571	21	0.0%	14	0.0%	-	0.0%
smoke_near	2581	2536	76	0.0%	76	0.0%	-	0.0%
Movie List	Frame Number	Smoke Frame Number	# alarms	False alarm rate	# alarms	False alarm rate	# alarms	False alarm rate
B1001	1469	0	32	2.1%	-	0.0%	7	0.5%
Lab001	1837	0	9	0.4%	-	0.0%	-	0.0%
Lab003	2587	0	30	1.2%	12	0.4%	98	3.8%
raw_highway1	440	0	-	0.0%	-	0.0%	-	0.0%
raw_highway2	500	0	-	0.0%	-	0.0%	41	8.8%

Smoke detection results of UE-Tunnel (2 smoke videos and 7 non-smoke videos) testing set.

Video Info.			C.Y. Lee and C.T. Lin (SVD V1.0)		This study (SVD V2.0)		Töreyin, et. al	
Movie List	Frame Number	Smoke Frame Number	Frame To Detect	False alarm rate	Frame To Detect	False alarm rate	Frame To Detect	False alarm rate
TunnelSmoke	6000	4640	46	0.0%	51	0.0%	72	3.0%
隧道煙霧	3872	943	19	0.0%	17	0.0%	19	0.0%
Movie List	Frame Number	Smoke Frame Number	# alarms	False alarm rate	# alarms	False alarm rate	# alarms	False alarm rate
TunnelTruck	5565	0	8	0.0%	2	0.0%	38	0.7%
隧道 1	4597	0	351	7.6%	40	0.9%	800	17.4%
隧道 2	4870	0	27	0.6%	-	0.0%	489	25.3%
隧道 1D	1777	0	-	0.0%	-	0.0%	25	2.2%
隧道 1N	2817	0	-	0.0%	-	0.0%	75	3.4%
隧道 2D	1936	0	-	0.0%	-	0.0%	204	10.7%
隧道 2N	2930	0	-	0.0%	-	0.0%	131	4.6%

Smoke detection results of Cetin (9 smoke videos and 2 non-smoke videos) testing set.

Video Info.			C.Y. Lee and C.T. Lin (SVD V1.0)		This study (SVD V2.0)		Töreyin, et. al	
Movie List	Frame Number	Smoke Frame Number	Frame To Detect	False alarm rate	Frame To Detect	False alarm rate	Frame To Detect	False alarm rate
sBtFence2	1400	1380	73	0.0%	48	0.0%	83	0.0%
sEmptyR1	483	302	14	0.0%	123	0.0%	0	0.0%
sEmptyR2.	342	253	60	0.0%	30	0.0%	17	0.0%
ShorterIsyamNight	1663	515	382	0.0%	378	0.0%	30	0.0%
sMoky	900	900	38	0.0%	30	0.0%	72	0.0%
sParkingLot	1726	1453	X	0.0%	32	0.0%	1130	0.0%
sWasteBasket	900	870	78	0.0%	62	0.0%	60	0.0%
sWindow	244	212	122	0.0%	-	0.0%	125	0.0%
sBtFence2	1400	1380	73	0.0%	48	0.0%	83	0.0%
Movie List	Frame Number	Smoke Frame Number	# alarms	False alarm rate	# alarms	False alarm rate	# alarms	False alarm rate
CarLights1	155	0	61	39.4%	-	0.0%	-	0.0%
CarLights2	160	0	8	5%	-	0.0%	-	0.0%

Smoke detection results of Visor (14 smoke videos) testing set.

Video Information			C.Y. Lee and C.T. Lin (SVD V1.0)		This study (SVD V2.0)		Töreyin, et. al	
Movie List	Frame Number	Smoke Frame Number	Frame To Detect	False alarm rate	Frame To Detect	False alarm rate	Frame To Detect	False alarm rate
visor_1196179837385_movie11_viper	1900	1148	56	0.0%	158	0.0%	64	4.1%
visor_1196343040120_movie12_viper	2342	1467	67	0.0%	128	0.0%	-	0.0%
visor_1196343142698_movie13_viper	2021	1285	68	0.0%	69	0.0%	-	0.0%
visor_1196343179807_movie14_viper	2148	1526	8	0.0%	74	0.0%	-	0.0%
visor_1197283983165_01_ballistic.avi	347	255	20	0.0%	25	0.0%	15	0.0%
visor_1197283985149_02_explosion.avi	210	160	54	0.0%	49	0.0%	13	0.0%
visor_1197283985415_03_burnout_contest.avi	2200	862	29	0.0%	63	0.0%	121	0.0%
visor_1197283980290_10_hangar	2952	2309	-	0.0%	32	0.0%	278	10.8%
visor_1197283990821_04_fumogeno1	3004	1974	56	0.0%	37	0.0%	949	3.3%
visor_1197284001212_05_fumogeno2	1834	1361	37	0.0%	97	0.0%	26	0.0%
visor_1197284006306_06_fumogeno3	2344	1392	38	0.0%	318	0.0%	0	0.0%
visor_1197284015696_07_fumogeno4	2023	1239	43	0.0%	101	0.0	33	12.8%
visor_1197284021149_08_fumogeno5	2150	1453	18	0.0%	108	0.0%	0	0.0%
visor_1197284028899_09_fumogeno6	1879	1327	38	0.0%	51	0.0%	36	0.0%